NASA Technical Memorandum 87041

The Generation of Capillary Instabilities by External Disturbances in a Liquid Jet

Stewart J. Leib
Lewis Research Center
Cleveland, Ohio

May 1985

NASA

TABLE OF CONTENTS

CHAPTER 1

INTRODUCTION

1.1 Liquid Jet Instability

The first theoretical study of the capillary (or surface tension) instability of a jet of liquid was carried out by Rayleigh (1878). He analyzed the linear stability of an inviscid, incompressible, infinitely long cylindrical jet (with plug flow velocity profile) to a spatially harmonic disturbance of the jet surface. Only axisymmetric modes were found to be unstable and the wavelength of the most unstable (temporally growing) mode was determined to be 4.51 . . . times the undisturbed jet diameter. The cutoff wavelength for unstable disturbances, below which the disturbance will decay in time, was found to be equal to the undisturbed jet circumference.

Later, Rayleigh (1892) included the effects of viscosity on the jet stability. He found that increasing the viscosity had the effect of increasing the wavelength of the most unstable mode. Since these studies, numerous investigators have studied the jet breakup process.

Most of the analyses treated the temporal instability problem. Lee (1974) used a one-dimensional, inviscid model to study the jet breakup process. Proceeding on the assumption that the axial velocity depends only on the axial coordinate he arrived at a simplified set of equations for momentum and mass conservation. The linearized equations thus obtained were solved in closed form while numerical solutions were obtained for the nonlinear analysis. Among the results obtained were the time for the jet to breakup (in both the linear and nonlinear cases) and the volume ratio of the satellite drops to the total drops (in the nonlinear analysis). In the range of parameters studied satellite drops were always found to occur.

While the temporal theory has received the most attention the actual jet breakup usually takes place as a result of spatially growing disturbances. This was recognized by Keller, Rubinow and Tu (1973) who, after making a transformation to a moving jet, solved the dispersion relation obtained by Rayleigh with real frequency while allowing the wavenumber to be complex. In this way spatially growing waves are obtained.

It was found by Keller et al. that the growth rates for the temporal and spatial instabilities are the same only in the infinite Weber number limit. Hence the results from the temporal theory can be applied as an approximation to a real jet only for large Weber numbers.

Pimbley (1976), used the one-dimensional model of Lee to treat a boundary value problem where the unstable disturbances grow with distance from the jet exit. He found that Lee's solution (after a transformation appropriate to a moving jet) was the infinite Weber number limit of the solution to his boundary value problem.

Experimental work has necessarily been concerned with spatially growing disturbances and the jet is seen to break into drops at some distance from the nozzle rather than after some period of time. The results obtained for the growth rates and jet breakup lengths have generally been converted for comparison with Rayleigh's (temporal) theory using the jet velocity.

Crane, Birch, and McCormack (1964) were able to obtain uniformly spaced and sized drops over a range of disturbance wavelengths which corresponded to the range predicted by Rayleigh's linear theory. The growth rates of disturbances of different wavelengths were determined and found to depart appreciably from the theoretical predictions of Rayleigh. The finite amplitude of the induced disturbances and consequent nonlinear effects were the reasons given for the differences. In support of this

a plot was given which shows that the growth rates in the experiment breaks away from the linear curve a short distance from the nozzle exit.

Donnelly and Glaberson (1966) performed experiments on liquid jets of water and glycerine-water solutions in air. Disturbances were induced on the jet by a nearby loudspeaker. Very clear stoboscopic flash photographs were taken of the jet breakup process showing the formation of the droplets. From these pictures the dispersion curve for the disturbances was determined. The spatial growth of the disturbances, as shown by the photographs, was converted to a temporal growth using the frequency of the forcing and the wavelength of the induced disturbance for comparison with Chandrasekhar's (1961) linear analysis (which was based on Rayleigh's analysis). The results were found to compare quite favorably. In light of the studies mentioned above this can probably be traced to the large value of the jet velocity compared with the capillary velocity (i.e., large Weber number) and the fact that a linear growth rate was found to persist to within one wavelength of the point at which drops begin to break off.

Using the glycerine-water solution the effect of viscosity on the stability of the jet was examined. It was found that increasing the viscosity had the effect of decreasing the growth rate, all other things being equal. These results agreed with Chandrasekhar's to within 20 percent. Small variations in the temperature of the jet, causing the viscosity to vary, was cited as one reason for the discrepancy.

A detailed review of the work done on liquid jet instability and a discussion of its applications to nozzle design has been made by McCarthy and Molloy (1974). Bogy (1979) has given an account of some more recent work concerning nonlinear effects on the jet breakup; in particular the formation of satellite drops.

1.2 Technological Applications

A number of technologies have evolved which make use of (and helped to motivate) the scientific studies touched on in the previous section. Perhaps the best known of these is the ink jet printer.

In such a printer the drops which are formed due to the jet instability are given a charge at the point where they break off from the jet. The charged drops pass through an electric field which causes them to be deflected from their original paths. The deflected drops then strike the paper and form characters. Details of the workings of such a system have been given by Kuhn and Meyers (1979).

It is easy to see that for such a system to perform properly the jet breakup and drop formation must be carefully controlled. A particular problem is the appearance of the small satellite drops which are observed to occur between the main drops. For this reason a significant effort has been made to understand this (nonlinear) phenomenon.

A more recent idea for exploiting the jet breakup process is in its use as a heat transfer device, the so-called liquid droplet radiator. Here a heated jet of fluid is shot out of a nozzle into a collector a certain distance downstream. As the jet travels between the nozzle and the collector (and breaks into drops) it radiates energy into the space around it. The fluid is then caught in the collector and circulated back through the system. The aim is to develop this type of system for use in space on satellites or spacecraft.

Some advantages to its use in space over more conventional systems are the large surface area to volume ratio of the drops, the relative ease of transporting into space a container of fluid over a network of pipes and its greater chances of surviving the impact of small particles floating through space.

A study of the feasibility of the liquid droplet radiator was made by Mattick and Hertzberg (1982). While their results showed promise, more work is needed before a practical system can be made.

We have cited two examples where the liquid capillary jet breakup process can be put to use. These examples illustrate the importance of understanding and being able to control the jet breakup.

1.3 Receptivity

It has been found in a number of problems in which a flow is subject to incident disturbances (Jones and Morgan (1972), Crighton and Leppington (1974), and Goldstein (1981)) that eigensolutions which grow exponentially downstream must be added to a particular solution in order to satisfy either edge requirements or causality (or both). The causality condition requires that the flow not respond to a disturbance before that disturbance is imposed. The edge condition which is usually specified is the Kutta condition that the velocity and pressure be finite at any edges or other singular points. The appropriateness of the Kutta condition has been examined by including viscous effects near a singular point. A review of work concerned with the Kutta condition has been given by Crighton (1985).

In one such study, Rienstra (1981) using some results from triple deck theory obtained by Brown and Daniels (1975), showed for a semi-infinite vortex sheet with a plane harmonic wave incident on it, that the solution satisfying the Kutta condition is obtained as the leading order term in the asymptotic expansion of the outer solution for the corresponding viscous problem. Hence the imposition of the Kutta condition in the inviscid solution is consistent with the detailed structure of the viscous flow near the edge.

The eigensolutions which are introduced into the solutions in this way contain terms which involve instability waves. The Kutta condition then provides a mechanism by which the external disturbances can couple to instability waves. A similar coupling occurs when causality is imposed. Since specific constant multiples of the eigensolution are needed to satisfy each of these conditions the amplitude of the instability waves is thereby specified.

The triggering of instability waves by external disturbances is the so-called receptivity problem (Morkovin (1969)). The aim of the study of receptivity is to determine the effectiveness of particular disturbances in exciting instability waves in a flow. One measure of this efficiency is the amplitude of the instability wave produced by the disturbance per unit amplitude of the forcing. This quantity is known as the coupling coefficient. Since the Kutta condition determines the amplitude of the instability wave we say that the Kutta condition completely specifies the receptivity problem. Similarly the causality condition can also be used to specify the receptivity problem. In some problems these conditions lead to the same result (Crighton and Leppington (1974)) while in others they do not (Goldstein (1981)). We will be addressing this question for the problem studied here.

1.4 Scope of the Present Work

The process of the breakup of a liquid jet begins at the nozzle exit where spatially growing capillary instabilities are excited by the external disturbance environment. The disturbances may be those which are coincidentally present in a facility or those due to a known forcing which is intentionally imposed on the jet. Since only the axisymmetric mode is unstable the jet deformation is varicose in nature (Rayleigh (1878)). At the point downstream of the exit where the amplitude of the

instability waves become equal to the original radius of the jet a drop of liquid is pinched off from the jet. Beyond this point the flow consists of a series of such drops possibly with a set of smaller drops (called satellite drops) occuring between the main drops. A simple schematic of this process is given in figure 1.1.

In applications such as those discussed in figure 1.2 it is necessary to be able to control the drop formation. In some cases for example it may be desired to produce drops of uniform size or to ellimate satellite drops. Control over the breakup process can be accomplished by imposing an appropriate external disturbance on the flow. Since the jet breakup process begins with instability waves the need to understand how an external disturbance effects the drop formation leads one to a consideration of the receptivity problem for a liquid jet.

In the present work we consider the inviscid, incompressible, parallel flow of a liquid jet emerging into a vacuum from a circular cylindrical nozzle subjected to a small, time harmonic disturbance. Specifically, this disturbance will take the form of a pulsating axial pressure gradient. Linearized equations for the fluctuations produced by this perturbation are solved subject to the kinematic and dynamic boundary conditions on the duct walls and free surface of the jet.

We will require that this "steady-state" (time-harmonic) solution be causal. That is, that it can develop as the long time response of the flow to a forcing started instantaneously at some initial time. Our goal is to determine when spatially growing instability waves can be excited by the external disturbance.

It will be seen that there are an infinite number of solutions to the problem outlined above. These solutions will differ in their behavior near the trailing edge of the duct. Out of these we will

choose the least singular one since this is the one which can be expected to match to an "inner" solution which takes viscosity into account (Van Dyke (1964)).

We begin in Chapter 2 with the general formulation of the problem. Physical variables are defined and the flow geometry illustrated. We then obtain the linearized differential equations and boundary conditions for the fluctuating variables.

In Chapter 3 we construct a causal solution to the forced problem using a method given by Briggs (1964). A brief description of the method is given in the appendix.

Under certain conditions the causal solution will involve a term which grows exponentially downstream. This term represents a Rayleigh instability wave. A major purpose for this study is to determine the amplitude of the instability wave relative to the amplitude of the forcing. This is the so-called "coupling coefficient".

At the end of Chapter 3 we write down a noncausal particular solution to the same equations and boundary conditions. We will find that this solution is singular at the trailing edge of the duct.

In Chapter 4 we construct an eigensolution to the problem and use it to eliminate the singularity in the noncausal particular solution so that the resulting solution satisfies the Kutta condition. This solution again involves instability waves and we can compute the coupling coefficient. The solution obtained in this way is compared with the causal solution.

Finally, in Chapter 5 we discuss the various solutions and summarize the results obtained.

CHAPTER 2

FORMULATION OF THE PROBLEM

2.1 Formulation

We consider the inviscid, incompressible, parallel flow of a liquid jet emerging from a semi-infinite circular duct of radius a into an evacuated region. The flow geometry and coordinate system used is shown in figure 2.1.

A steady base flow (which satisfies the inviscid equations of motion for any choice of $U(r)$

$$\begin{aligned} \underset{\sim}{U} &= (U(r),\ 0) \\ P &= C = \text{constant} \end{aligned} \tag{2.1}$$

is subjected to a small, time harmonic, axisymmetric perturbation.

Assuming the equations can be linearized the fluctuations due to this disturbance will likewise be harmonic in time and we write them as

$$(u',v',p') = e^{-i\omega t}\ (u'(x,r),\ v'(x,r),\ p'(x,r)) \tag{2.2}$$

where ω is the frequency of the disturbance.

We write the instantaneous variables as

$$\begin{aligned} u^T &= U + u' \\ v^T &= v' \\ p^T &= p' + C \end{aligned} \tag{2.3}$$

The instantaneous flow variables are governed by Euler's equation for an inviscid fluid

$$\rho \left[\frac{\partial \underset{\sim}{u}^T}{\partial t} + (\underset{\sim}{u}^T \cdot \nabla)\ \underset{\sim}{u}^T \right] = -\nabla p^T \tag{2.4}$$

and the incompressible continuity equation

$$\nabla \cdot \underset{\sim}{u}^T = 0 \tag{2.5}$$

The kinematic boundary condition on the solid duct wall is

$$v^T(x,a,t) = 0; \quad -\infty < x < 0 \qquad (2.6)$$
$$0 < t < \infty$$

The perturbed free surface of the jet can be described by an equation of the form

$$r = \zeta(x,t) + a \qquad (2.7)$$

where ζ is the displacement of the surface from its undisturbed position.

On the free surface we have the kinematic boundary condition that particles on the surface move with the surface. That is,

$$v^T(x,\zeta + a,t) = \frac{D\zeta}{Dt} \qquad (2.8)$$

where D/Dt is the convective derivative

$$\frac{D}{Dt} = \frac{\partial}{\partial t} + u^T(\zeta + a)\frac{\partial}{\partial x} \qquad (2.9)$$

In the absence of viscosity the dynamic condition at the free surface requires that surface tension forces balance pressure forces. This condition can be written as

$$P^T(x,\zeta + a,t) = \gamma\left(\frac{1}{R_1} + \frac{1}{R_2}\right) \qquad (2.10)$$

where γ is the surface tension and R_1 and R_2 are the principal radii of curvature of the surface at position x and time t (Landau and Lipshitz (1959) p. 231).

Substituting equation (2.3) into equations (2.4) to (2.6) and linearizing for small disturbances we get

$$\rho\left[\frac{\partial u'}{\partial t} + U(r)\frac{\partial u'}{\partial x} + \frac{dU(r)}{dr}v'\right] = -\frac{\partial p'}{\partial x} \qquad (2.11)$$

$$\rho\left[\frac{\partial v'}{\partial t} + U(r)\frac{\partial v'}{\partial x}\right] = -\frac{\partial p'}{\partial r} \qquad (2.12)$$

$$\nabla \cdot \underset{\sim}{u}' = 0 \qquad (2.13)$$

$$v'(x,a,t) = 0 \qquad -\infty < x < 0 \qquad (2.14)$$

Since we have assumed that the disturbances are small, the displacement of the surface from its original position will be small. We can then expand the boundary conditions for $x > 0$ about $r = a$ for $\zeta \ll 1$. This gives

$$v'(x,a,t) = \frac{\partial \zeta}{\partial t} + U(a) \frac{\partial \zeta}{\partial x} \qquad 0 < x < \infty \qquad (2.15)$$

for the kinematic condition and

$$p'(x,a,t) = -\gamma \left(\frac{\zeta}{a^2} + \frac{\partial^2 \zeta}{\partial x^2} \right) \qquad 0 < x < \infty \qquad (2.16)$$

for the dynamic condition when the disturbances are axisymmetric (Lamb (1945) p. 473). Note that in equation (2.16) we have set $C = \gamma/a$ which is the equilibrium condition when there is no surface displacement.

We wish to determine the solution to the above problem for the particular case of a disturbance corresponding to a time harmonic axial pressure gradient $-P_o' e^{-i\omega t}$ where P_o' is a constant.

Boundary value problems with discontinuous boundary conditions such as we have here can be solved by the Wiener-Hopf method (Noble (1958), Roos (1969)). This method makes use of the analytic continuation of unilateral Fourier transforms into the complex plane. We make use of this method in the present work.

CHAPTER 3

FORCED JET SOLUTION

3.1 Introduction

Since the present formulation is linear we may obtain the solution to the forced jet problem by superposition.

In particular, we first consider the flow in a doubly infinite circular duct subject to an axial pressure gradient $-P_o' e^{-i\omega t}$ where P_o' is a constant. The solution to the doubly infinite duct problem will satisfy the differential equations (2.11) to (2.15), the boundary condition on the solid duct wall (eq. (2.14)) and the condition that at upstream infinity there is only a time harmonic pulsation of the flow due to the imposed pressure gradient. The two free surface conditions (eqs. (2.15) and (2.16)) however cannot be satisfied by this solution. For this reason we construct another solution to equations (2.11) to (2.13) which corrects the doubly infinite duct solution for the presence of the free surface and which vanishes as $x \to -\infty$ so that the upstream boundary condition remains satisfied.

In this way then the solution to the forced semi-infinite jet problem is obtained.

3.2 Doubly Infinite Circular Duct

We impose a time harmonic axial pressure gradient $\partial P^D/\partial x = -P_o' e^{-i\omega t}$ on the flow in a doubly infinite circular duct and seek solutions of the form

$$\underset{\sim}{u}^D(x,r,t) = \hat{\underset{\sim}{u}}^D(r)\, e^{i(\lambda x - \omega t)} \tag{3.1}$$

Since p^D is a function of x and t only equation (2.12) gives that $\hat{v}^D(r) \equiv 0$. In particular the kinematic boundary condition on the solid duct walls is identically satisfied. In order to satisfy

equation (2.11) we set $\lambda = 0$ and $\hat{u}^D(r) = iP_o'/\rho\omega$ a constant. Hence the solution to this problem becomes

$$\begin{aligned} p^D(x,t) &= -P_o' x e^{-i\omega t} + P_o e^{-i\omega t} \\ v^D(x,t) &\equiv 0 \\ u^D(x,t) &= \frac{iP_o'}{\rho\omega} e^{-i\omega t} \end{aligned} \tag{3.2}$$

for all x where P_o is the level of the pressure fluctuation at $x = 0$ which will be determined as part of the solution.

From equation (3.2) we can see that the boundary conditions of equations (2.15) and (2.16) are not satisfied by this solution. We next construct a solution to equations (2.11) to (2.13) which will correct equation (3.2) at the free surface of the jet.

3.3 Semi-infinite Jet

In order to correct equations (3.2) for the presence of the free surface we will seek functions $\tilde{\underset{\sim}{u}}(x,r,t)$, $\tilde{\zeta}(x,t)$ and $\tilde{p}(x,r,t)$, which satisfy equations (2.11) to (2.14), such that $\underset{\sim}{u}^D + \tilde{\underset{\sim}{u}}$ and $p^D + \tilde{p}$ satisfy the satisfy the boundary conditions for $x > 0$ (eqs. (2.15) and (2.16)).

Using equation (3.2) in equations (2.57) and (2.16) we write

$$\tilde{v}(x,a,t) = \left(\frac{\partial}{\partial t} + U(a)\,\frac{\partial}{\partial x}\right)\tilde{\zeta}(x,t) \tag{3.3}$$

and

$$\tilde{p}(x,a,t) = P_o' x e^{-i\omega t} - P_o e^{-i\omega t} - \gamma\left(\frac{1^2}{a^2} + \frac{\partial}{\partial x^2}\right)\tilde{\zeta}(x,t) \tag{3.4}$$

for $x > 0$.

Then the boundary value problem which determines the desired functions is

$$\rho\left[\frac{\partial \tilde{u}}{\partial t} + U(r)\,\frac{\partial \tilde{u}}{\partial x} + U'(r)\,\tilde{v}\right] = -\frac{\partial \tilde{p}}{\partial x} \tag{3.5}$$

$$\rho\left[\frac{\partial \tilde{v}}{\partial t} + U(r)\,\frac{\partial \tilde{v}}{\partial x}\right] = -\frac{\partial \tilde{p}}{\partial r} \tag{3.6}$$

$$\nabla \cdot \tilde{\underset{\sim}{u}} = 0 \tag{3.7}$$

$$\tilde{v}(x,a,t) = 0 \qquad -\infty < x < 0 \tag{3.8}$$

$$\tilde{u}(x,r,t) \to 0 \quad \text{as} \quad x \to -\infty \tag{3.8}$$

together with equations (3.3) and (3.4). A boundary value problem such as that above with discontinuous boundary conditions can be solved by Fourier transforms using the method of Wiener and Hopf.

Since for incompressible flow the absolute level of the pressure fluctuations does not vanish at infinity but is felt for all x $-\infty < x < \infty$ we have subtracted it out from the pressure above so that the Fourier transform of p will exist in the usual sense.

We will seek solutions of the form

$$(\tilde{u},\tilde{v},\tilde{p},\tilde{\zeta}) = (u(x,r),\ v(x,r),\ p(x,r),\ \zeta(x))\ e^{-i\omega t} \tag{3.9}$$

where the functions u, v, p, and ζ are sufficiently well behaved at infinity so that their Fourier transforms in x exist. These are defined as

$$\hat{u}(k,r) = \frac{1}{2\pi}\int_{-\infty}^{\infty} u(x,r)e^{-ikx}\,dx \tag{3.10}$$

etc.

The Wiener-Hopf technique makes use of the analytic continuation of half range Fourier transforms into the complex plane. These unilateral transforms are defined as

$$\hat{u}_{+}(k,r) = \frac{1}{2\pi}\int_{-\infty}^{0} u(x,r)e^{-ikx}\,dx \tag{3.11}$$

and

$$\hat{u}_-(k,r) = \frac{1}{2\pi}\int_0^\infty u(x,r)e^{-ikx}\,dx \tag{3.12}$$

The integral in equation (3.11) can be shown to converge uniformly in any closed and bounded subset of the upper half plane (Im k > 0) and hence represents an analytic function in the upper half plane (Roos (1969)). Likewise, equation (3.12) represents a function which is analytic in the lower half plane. Along the real axis we have

$$\hat{u}(k,r) = \hat{u}_+(k,r) + \hat{u}_-(k,r) \tag{3.13}$$

Similar relations can be written down for the other variables.

With the above definitions we Fourier transform equations (3.5) to (3.7) and obtain

$$\rho i(U(r)k - \omega)\hat{u}(k,r) + \rho U'(r)\hat{v}(k,r) = -ik\hat{p}(k,r) \tag{3.14}$$

$$\rho i(U(r)k - \omega)\hat{v}(k,r) = -\frac{d\hat{p}(k,r)}{dr} \tag{3.15}$$

$$ik\hat{u}(k,r) + \frac{\hat{v}(k,r)}{r} + \frac{d\hat{v}(k,r)}{dr} = 0 \tag{3.16}$$

Applying the half range transforms to the boundary conditions (eqs. (3.3), (3.4), and (3.8)) and noting that $\zeta(0,t) = 0$ we can write

$$\hat{v}_+(k,a) = 0 \tag{3.17}$$

$$\hat{v}_-(k,a) = i(U(a)k - \omega)\hat{\zeta}_- \tag{3.18}$$

$$\hat{p}_-(k,a) = \frac{-P_o'}{2\pi(k - i\epsilon^*)^2} + \frac{P_o}{2\pi i(k - i\epsilon^*)} + \gamma\left(k^2 - \frac{1}{a^2}\right)\hat{\zeta}_-(k) + \frac{\gamma\zeta'(0)}{2\pi} \tag{3.19}$$

In equation (3.19) we have added a small amount of damping $e^{i\epsilon^* x}$ for $x > o$ to the forcing terms so that the Fourier transform will

exist. The damping factor ϵ^* will be set equal to zero at the end of the analysis.

Equations (3.14) to (3.16) can be combined to arrive at Rayleigh's equation for $\hat{v}$ which becomes

$$\left(U(r) - \frac{\omega}{k}\right)\left[\left(\hat{v}'(k,r) + \frac{\hat{v}(k,r)}{r}\right)' - k^2\hat{v}(k,r)\right] - r\left(\frac{U'(r)}{r}\right)'\hat{v}(k,r) = 0 \tag{3.20}$$

for an arbitrary base flow profile $U(r)$. In equation (3.20) $'$ means differentiation with respect to r.

In the following we will take

$$U(r) = U_o\left(1 - b\,\frac{r^2}{a^2}\right); \quad 0 \le b \le 1 \tag{3.21}$$

where U_o is a constant. Using the parameter b we can get results for a range of profiles from plug flow to Hagen-Poiseuille flow.

Note that for this family of profiles

$$\frac{1}{r}\frac{d}{dr}\left[\frac{U'(r)}{r}\right] = 0 \tag{3.22}$$

With equations (3.21) and (3.22), equation (3.20) becomes

$$\hat{v}''(k,r) + \frac{1}{r}\hat{v}'(k,r) - \left(k^2 + \frac{1}{r^2}\right)\hat{v}(k,r) = 0 \tag{3.23}$$

Equation (3.23) is the modified Bessel equation of order one. Hence we can write

$$\hat{v}(k,r) = A(k)\, I_1(kr) + B(k)\, K_1(kr) \tag{3.24}$$

where I_1 and K_1 are the modified Bessel functions of the first and second kind, respectively.

In order for the solution to be bounded at $r = 0$ we must have $B(k) = 0$ so that

$$\hat{v}(k,r) = A(k)\, I_1(kr) \tag{3.25}$$

The function $A(k)$ is determined from the boundary conditions by the Wiener-Hopf technique.

From equations (3.13), (3.17), and (3.25) we can write

$$\hat{v}(k,a) = A(k)I_1(ka) = \hat{v}_-(k,a) \tag{3.26}$$

and

$$\hat{v}'(k,a) = A(k)kI_1'(ka) = \hat{v}_+'(k,a) + \hat{v}_-'(k,a) \tag{3.27}$$

for k along the real axis. (In eq. (3.27) $I_1'(ka) = d/d(ka)\, I_1(ka)$).

Eliminating $A(k)$ from equations (3.26) and (3.27) gives

$$\hat{v}_-(k,a) = \frac{I_1(ka)}{kI_1'(ka)}\left[\hat{v}_+'(k,a) + \hat{v}_-'(k,a)\right] \tag{3.28}$$

The boundary conditions (eqs. (3.18) and (3.19)) can be used to eliminate $\hat{\zeta}_-$ to get

$$\hat{p}_-(k,a) = \frac{-P_0'}{2\pi(k - i\varepsilon^*)^2} + \frac{P_0}{2\pi i(k - i\varepsilon^*)} + \frac{i\gamma\left(k^2 - \frac{1}{a^2}\right)}{[\omega - kU(a)]}\hat{v}_-(k,a) + \frac{\gamma\zeta'(0)}{2\pi} \tag{3.29}$$

Writing equation (3.14) at $r = a$ using equation (3.29) and the fact that $\hat{p}(k,a) = \hat{p}_+(k,a) + \hat{p}_-(k,a)$ along the real axis gives

$$i\rho[U(a)k - \omega]\,\hat{u}(k,a) + \rho U'(a)\,\hat{v}(k,a) = -ik\left[\hat{P}_+(k,a) - \frac{P_0'}{2\pi(k - i\varepsilon^*)^2}\right.$$

$$\left. + \frac{P_0}{2\pi i(k - i\varepsilon^*)} + \frac{i\gamma\left(k^2 - \frac{1}{a^2}\right)}{[\omega - kU(a)]}\hat{v}_-(k,a) + \frac{\gamma\zeta'(0)}{2\pi}\right] \tag{3.30}$$

Writing equation (3.16) at $r = a$ and using equations (3.26) and (3.28) we get

$$ik\,\hat{u}(k,a) = -\hat{v}_-(k,a)\left[\frac{1}{a} + \frac{kI_1'(ka)}{I_1(ka)}\right] \tag{3.31}$$

Substituting equations (3.26) and (3.31) into equation (3.30) and rearranging gives

$$\chi(k)(k - i\varepsilon^*)^2 \hat{v}_-(k,a) + ik^2(k - i\varepsilon^*)^2 \hat{p}_+(k,a) = \frac{ik^2 P_0'}{2\pi} - \frac{k^2(k - i\varepsilon^*)P_0}{2\pi} - \frac{i\gamma k^2(k - i\varepsilon^*)^2\zeta'(0)}{2\pi} \qquad (3.32)$$

where

$$\chi(k) = \frac{1}{[\omega - kU(a)]}\left\{\rho[\omega - kU(a)]^2\left[\frac{1}{a} + \frac{kI_1'(ka)}{I_1(ka)}\right] + \rho U'(a)k[\omega - kU(a)] + \gamma k^2\left(\frac{1}{a^2} - k^2\right)\right\} \qquad (3.33)$$

The key to the success of the Wiener-Hopf technique lies in finding a factorization for $\chi(k)$ such that

$$\chi(k) = \frac{\chi_+(k)}{\chi_-(k)} \qquad (3.34)$$

where χ_+ is analytic for $\text{Im } k > 0$ and χ_- is analytic for $\text{Im } k < 0$.

Formally the Wiener-Hopf equation can be written as

$$\frac{(k - i\varepsilon^*)^2 \hat{v}_-(k,a)}{\chi_-(k)} + \frac{ik^2(k - i\varepsilon^*)^2\hat{P}_+(k,a)}{\chi_+(k)} = \left[\frac{ik^2 P_0'}{2\pi} - \frac{k^2(k - i\varepsilon^*)P_0}{2\pi} - \frac{i\gamma k^2(k - i\varepsilon^*)^2\zeta'(0)}{2\pi}\right]\frac{1}{\chi_+(k)} \qquad (3.36)$$

Due to the nature of the kernal function $\chi(k)$, specifically that it is meromorphic, the factorization (eq. (3.34)) can be performed in a simple way by making use of the Weierstrass factorization theorem (Roos (1969)). As mentioned in the introduction, the solution we are seeking is the least singular causal solution. In view of this we will construct

our factorizations so as to be consistent with the requirements of causality.

3.4 Factorization of the Kernal Function and Inhomogeneous Terms

3.4.1 Causality

A general method for obtaining a causal response of a system to an impulsively started forcing has been given by Briggs (1964). Our concern here is that our "steady state" (time harmonic) solution be the long-time response of the flow which develops in a causal way from a forcing which was initiated at some time, say $t = 0$. The causality condition is that there is no response before the forcing is "turned on", that is for $t < 0$.

So as not to disrupt the discussion of the analysis a description of the main points of Briggs' method is deferred to an appendix. At this time we merely point out that a causal solution can be obtained by solving the problem with the frequency ω having a large positive imaginary part. The (causal) solution for real ω is then obtained by analytic continuation.

The requirement that $\mathrm{Im}\,\omega$ be large has no effect on the algebra leading to equation (3.32). The factorization of the kernal function, however, is effected in a very important way. We now proceed to determine this factorization.

3.4.2 The Weierstrass Factorization Formula

The Weierstrass factorization formula allows us to write an entire function with simple zeros as an infinite product (Roos (1969) p. 174)

$$\tilde{E}(Z) = \tilde{E}(o)\, e^{Z\, d/dZ\{\log[\tilde{E}(Z)]\}_{Z=0}} \prod_{n=1}^{\infty} \left(1 - \frac{Z}{a_n}\right) e^{Z/a_n} \qquad (3.37)$$

where the a_n are the (simple and nonzero) zeros of $\tilde{E}(Z)$ provided

that

$$\sum_{n=1}^{\infty}\left(\frac{R}{a_n}\right)^2 < \infty \tag{3.38}$$

for any $R > 0$ (Conway (1978) p. 170).

If we represent the zeros of $\tilde{E}$ in the upper half plane by a_n^U and those in the lower half plane by a_n^L we can rewrite equation (3.37) as

$$\tilde{E}(Z) = \tilde{E}(o)\, e^{Z[\log[\tilde{E}(Z)]]'_{Z=0}} \prod_{n=1}^{\infty}\left(1 - \frac{Z}{a_n^U}\right)e^{Z/a_n^U} \cdot \prod_{n=1}^{\infty}\left(1 - \frac{Z}{a_n^L}\right)e^{Z/a_n^L} \tag{3.39}$$

We can then define functions $\tilde{E}_+$ and $\tilde{E}_-$ such that

$$\tilde{E}(Z) = \frac{\tilde{E}_+(Z)}{\tilde{E}_-(Z)} \tag{3.40}$$

where

$$\tilde{E}_+(Z) = e^{\phi(Z)} \prod_{n=1}^{\infty}\left(1 - \frac{Z}{a_n^L}\right)e^{Z/a_n^L} \tag{3.41}$$

and

$$\tilde{E}_-(Z) = \frac{e^{\phi(Z)}\, e^{-Z[\log[\tilde{E}(Z)]]'_{Z=0}}}{\tilde{E}(o) \prod_{n=1}^{\infty}\left(1 - \frac{Z}{a_n^U}\right)e^{Z/a_n^U}} \tag{3.42}$$

In equations (3.41) and (3.42) $\tilde{E}_+(Z)$ is analytic and nonzero in the upper half plane and $\tilde{E}_-(Z)$ is analytic and nonzero in the lower half plane. $d(Z)$ is an entire function chosen so that $\tilde{E}_+$ is algebraic at infinity (Noble (1985) p. 15).

To arrive at the desired factorization for our Kernel function we first write $\chi(k)$ in dimensionless form and group terms as

$$\chi(\tilde{x}) = \frac{1}{[\Omega - \tilde{x}(1 - b)]}\left[\frac{\tilde{x}}{I_1(\tilde{x})}\right] \cdot \left[\left(\frac{I_1(\tilde{x})}{\tilde{x}} + I_1'(\tilde{x})\right)[\Omega - \tilde{x}(1 - b)]^2 + \frac{I_1(\tilde{x})}{\tilde{x}} \frac{\tilde{x}^2(1 - \tilde{x}^2)}{\beta^2} - \frac{I_1(\tilde{x})}{\tilde{x}} 2b\tilde{x}[\Omega - \tilde{x}(1 - b)]\right]\frac{\rho U_0}{a} \qquad (3.43)$$

or

$$\chi(\tilde{x}) = \frac{1}{[\Omega - \tilde{x}(1 - b)]} \frac{F_1(\tilde{x})}{F_2(\tilde{x})} \frac{\rho U_0}{a} \qquad (3.44)$$

where

$$F_1(\tilde{x}) = \left(\frac{I_1(\tilde{x})}{\tilde{x}} + I_1'(\tilde{x})\right)[\Omega - \tilde{x}(1 - b)]^2 + \frac{\tilde{x}^2(1 - \tilde{x}^2)}{\beta^2} \frac{I_1(\tilde{x})}{\tilde{x}} - 2b\tilde{x}[\Omega - \tilde{x}(1 - b)] \frac{I_1(\tilde{x})}{\tilde{x}} \qquad (3.45)$$

and

$$F_2(\tilde{x}) = \frac{I_1(\tilde{x})}{\tilde{x}} \qquad (3.46)$$

In equations (3.43) to (3.46) we have defined dimensionless quantities as $\Omega = \omega a/U_0$, $\tilde{x} = ka$ and $\beta^2 = \rho a U_0^2/\gamma$ where Ω is the Strouhal number and β^2 is the Weber number and we have used equation (3.21) for $U(r)$. Since the imaginary part of ω (and hence of Ω) is positive the term $1/[\Omega - \chi(1 - b)]$ is analytic in the lower half plane. The entire functions F_1 and F_2 can be factored using the Weierstrass formula.

Consider first the function F_2. Let $\tilde{\beta}_n$ be the zeros of F_2 (which are the zeros of I_1) in the upper half plane. Since F_2 is an even function of $\tilde{x}$ the zeros in the lower half plane are simply $-\tilde{\beta}_n$. All of the zeros of F_2 are pure imaginary. If $\tilde{x} = i\sigma$ is pure imaginary we can rewrite F_2 as (Abramowitz and Stegun (1964)).

$$F_2(i\sigma) = \frac{I_1(i\sigma)}{i\sigma} = \frac{J_1(\sigma)}{\sigma} \tag{3.47}$$

As $\sigma \to \infty$ we have

$$J_1(\sigma) \sim \frac{2}{\pi\sigma}\left(\cos \sigma - \frac{3\pi}{4}\right) \tag{3.48}$$

Since the zeros of the cosine grow like n as $n \to \infty$, the relation (eq. (3.38)) is satisfied and equation (3.37) can be applied.

We can easily find that

$$F_2(0) = \frac{1}{2} \tag{3.49}$$

and

$$\frac{d}{d\tilde{x}}\left[\log[F_2(\tilde{x})]\right]_{\tilde{x}=0} = 0 \tag{3.50}$$

By equation (3.39) then we can write

$$F_2(\tilde{x}) = \frac{1}{2}\prod_{n=1}^{\infty}\left(1 - \frac{\tilde{x}}{\tilde{\beta}_n}\right)\left(1 + \frac{\tilde{x}}{\tilde{\beta}_n}\right)e^{\tilde{x}(1/\tilde{\beta}_n - 1/\tilde{\beta}_n)} \tag{3.51}$$

The function $F_1(\tilde{x})$ can be handled in a similar way. Let ξ_m be the zeros of F_1 in the upper half plane and ζ_m those in the lower half plane. Asymptotically the zeros of F_1 becomes just the zeros of I_1. In particular they grow like m as $m \to \infty$. We can evaluate the constants needed in equation (3.37) as

$$F_1(0) = \Omega^2 \tag{3.52}$$

and

$$\frac{d}{d\tilde{x}}\left[\log[F_1(\tilde{x})]\right]_{\tilde{x}=0} = \frac{b-2}{\Omega} \tag{3.53}$$

Then using equation (3.37)

$$F_1(\tilde{x}) = \Omega^2 \, e^{\frac{\tilde{x}(b-2)}{\Omega}} \prod_{m=1}^{\infty} \left(1 - \frac{\tilde{x}}{\zeta_m}\right)\left(1 - \frac{\tilde{x}}{\xi_m}\right) e^{\tilde{x}[1/\zeta_m + 1/\xi_m]} \tag{3.54}$$

Combining equations (3.44), (3.51), and (3.54) we can rewrite the kernel function as

$$\chi(\tilde{x}) = \frac{2\Omega^2 \, e^{\tilde{x}(b-2)/\Omega} \prod_{m=1}^{\infty} \left(1 - \frac{\tilde{x}}{\zeta_m}\right)\left(1 - \frac{\tilde{x}}{\xi_m}\right) e^{\tilde{x}(1/\zeta_m + 1/\xi_m)} \left(\frac{\rho U_o}{a}\right)}{[\Omega - \tilde{x}(1-b)] \prod_{n=1}^{\infty} \left(1 - \frac{\tilde{x}}{\tilde{\beta}_n}\right)\left(1 + \frac{\tilde{x}}{\tilde{\beta}_n}\right) e^{\tilde{x}(1/\tilde{\beta}_n - 1/\tilde{\beta}_n)}} \tag{3.55}$$

Now let $\tilde{\zeta}_m = -\zeta_m$ and define

$$\chi_+(\tilde{x}) = \frac{\prod_{m=1}^{\infty} \left(1 + \frac{\tilde{x}}{\tilde{\zeta}_m}\right) e^{-\tilde{x}/\tilde{\zeta}_m}}{\prod_{n=1}^{\infty} \left(1 + \frac{\tilde{x}}{\tilde{\beta}_n}\right) e^{-\tilde{x}/\tilde{\beta}_n}} e^{\tilde{\phi}(\tilde{x})} \tag{3.56}$$

and

$$\chi_-(\tilde{x}) = \frac{[\Omega - \tilde{x}(1-b)] \prod_{n=1}^{\infty} \left(1 - \frac{\tilde{x}}{\tilde{\beta}_n}\right) e^{\tilde{x}/\tilde{\beta}_n}}{\left(\frac{\rho U_o}{a}\right) 2\Omega^2 \, e^{\tilde{x}(b-2)/\Omega} \prod_{m=1}^{\infty} \left(1 - \frac{\tilde{x}}{\xi_m}\right) e^{\tilde{x}/\xi_m}} e^{\tilde{\phi}(\tilde{x})} \tag{3.57}$$

so that

$$\chi(\tilde{x}) = \frac{\chi_+(\tilde{x})}{\chi_-(\tilde{x})} \tag{3.58}$$

Equations (3.56) to (3.58) then give the desired factorization.

In order to determine the function $\tilde{\phi}(\tilde{x})$ in equations (3.56) and (3.57) we need to determine the asymptotic behavior of the infinite products in these equations. An asymptotic expansion for the infinite products, with $\tilde{x}$ in the upper half plane, has been given by Noble (p. 128). We can apply this expansion directly once we know the asymptotic form of the roots $\tilde{\beta}_n$ and $\tilde{\zeta}_m$.

From equation (3.48) we can find that

$$\tilde{\beta}_n \sim i\pi(n + n_o) + \frac{i\pi}{4} \tag{3.59}$$

as $n \to \infty$ where n_o is some integer.

Recall that the zeros of F_1 approach those of F_2 as $\tilde{x} \to \infty$. The asymptotic form of ζ_m then is formally the same as equation (3.59) so we can write

$$\tilde{\zeta}_m \sim i\pi(m + m_o) + \frac{i\pi}{4} \tag{3.60}$$

as $m \to \infty$ where m_o is some integer. The difference between the integers m_o and n_o will be equal to the number of roots in the lower half plane which are left over after we identify the set of roots of F_1 which can be put into a one-one correspondence with the roots of F_2. The roots of these two functions were determined numerically and it was found that each of the roots of F_2 could be associated with a root of F_1 with four roots of F_1 left over. We will denote the number of these four roots which lie in the lower half plane by ℓ. The numerical value of ℓ may be a function of the particular values of the physical parameters being considered. Now since there are ℓ roots of

F_1 in the lower half plane beyond those which can be associated with roots of F_2 we must have $m_o = n_o - \ell$ in equation (3.60). Then the correct asymptotic form for ζ_n is

$$\tilde{\zeta}_n \sim i\pi(n + n_o) + \frac{i\pi}{4}(1 - 4\ell) \tag{3.61}$$

With equations (3.59) and (3.61) we can write the asymptotic expansion for χ_+ as (Noble, p. 128)

$$\chi_+(\tilde{x}) \sim \exp\left\{\tilde{\phi}(\tilde{x}) - \left(\frac{\tilde{x}}{i\pi} + \frac{1}{4}(1 - 4\ell) + \frac{1}{2}\right) \cdot \log\left(\frac{\tilde{x}}{i\pi} + \frac{1}{4}(1 - 4\ell) + 1\right)\right.$$
$$\left. + \left(\frac{\tilde{x}}{i\pi} + \frac{1}{4} + \frac{1}{2}\right) \cdot \log\left(\frac{\tilde{x}}{i\pi} + \frac{1}{4} + 1\right) + \tilde{x} \sum_{n=1}^{\infty}\left(\frac{1}{\tilde{\beta}_n} - \frac{1}{\tilde{\zeta}_n}\right)\right\} \tag{3.62}$$

If we choose

$$\tilde{\phi}(\tilde{x}) = -\tilde{x} \sum_{n=1}^{\infty}\left(\frac{1}{\tilde{\beta}_n} - \frac{1}{\tilde{\zeta}_n}\right) \tag{3.63}$$

we will have that

$$\chi_+(\tilde{x}) \sim \tilde{x}^{\ell} \tag{3.64}$$

as $\tilde{x} \to \infty$.

A numerical study was made of the "left over" zeros of $F_1(\tilde{x})$ over a range of the physical parameters in order to determine the factor ℓ. The results of that study are now described.

3.4.3 Numerical Results for the Roots

Of the four roots we are considering here two are real and two are complex conjugates when $\mathrm{Im}\ \Omega = 0$. Causality considerations require that we determine the position of these roots when $\mathrm{Im}\ \Omega$ becomes large. The movement of the roots of $F_1(x)$ as $\mathrm{Im}\ \Omega$ is increased from zero was studied numerically for a number of combinations of Strouhal number, Weber number and mean velocity profile.

For each mean profile there is a range of Weber number and Strouhal number for which the four roots move as shown in figure 3.1. This sketch shows the movement of the roots as $\mathrm{Im}\ \Omega$ is varied. The important thing to note about this figure is the movement of the complex root which lies in the lower half plane when $\mathrm{Im}\ \Omega = 0$. For fixed profile and Weber number there is a range of $\mathrm{Re}\ \Omega$ (i.e., the Strouhal number) for which this root crosses the real axis and moves into the upper half plane as $\mathrm{Im}\ \Omega$ is increased as shown in figure 3.1. This crossing of the real axis of a complex root is the criterion for the existence of spatially growing waves in the causal solution (Briggs (1964)). The range of $\mathrm{Re}\ \Omega$ for which this crossing occurs then corresponds to the Strouhal number range over which the flow supports instability waves. Outside of this range the flow is stable. For a given mean profile and Weber number the range of Strouhal number over which the flow supports instability waves can be determined by finding the range of $\mathrm{Re}\ (\Omega)$ over which this root crosses the real axis. The locus of this root as a function of (complex) Strouhal number was determined for a number of combinations of mean profile and Weber number. The results of the computations are shown in figures 3.2 to 3.19.

For the plug flow profile ($b = 0$) the cutoff Strouhal number (above which the flow is stable) was found to be equal to one independent of the value of the Weber number in the range computed. Results obtained for other profiles ($b \neq 0$) indicate that for fixed b the range of Strouhal number over which instability waves exist decreases with increasing Weber number (see figs. 3.9 to 3.14 and 3.15 to 3.19). Additionally, for a given Weber numer, this Strouhal number range was found to decrease quite rapidly with increasing b. In fact when the profile parameter

was increased beyond 0.5 no roots were found which correspond to instability waves for the range of Weber number reported here.

In the course of studying the movement of these roots another situation was discovered. For the plug profile when $\beta^2 < 5$ the roots move in the way illustrated in figure 3.20. Notice that in this situation two roots which appear in opposite half planes when $\text{Im}\ \Omega >> 1$ swap their positions for $\text{Im}\ \Omega = 0$ when the Strouhal number is increased beyond a certain value. Using the criterion of Briggs (1964) this indicates that the flow is absolutely unstable for these Weber numbers. That is, disturbances grow in time at every point in space. When the flow is absolutely unstable it is no longer appropriate to consider spatially growing instability waves.

For the purposes of this study, since we are interested in the generation of spatially growing Rayleigh instabilities, we will confine our attention to the parameter ranges for which the flow is convectively unstable. In this range the roots move as in figure 3.1 so that $\ell = 2$.

With the position of the roots of F_1 thus determined the factorization of the kernal function is complete. It remains only to factor the inhomogeneous terms. This is particularly simple in this case.

From equation (3.36) we can see that the inhomogeneous terms (those on the right) are by inspection "plus" functions. We can now proceed to solve the Wiener-Hopf equation (eq. (3.36)).

3.5 Solution of the Wiener-Hopf Equation

"Finding the solution" in problems of this type consists of finding expressions for both $\hat{v}_-$ and $\hat{p}_+$. This is accomplished by using analytic continuation arguments along with Liouville's theorem on entire functions.

We begin by rewriting equation (3.36) as

$$\frac{\hat{v}_-(k,a)(k - i\varepsilon^*)^2}{\chi_-(k)} = \frac{-ik^2(k - i\varepsilon^*)^2\hat{P}_+(k,a)}{\chi_+(k)} + \frac{ik^2P_0'}{2\pi\chi_+(k)} - \frac{k^2(k - i\varepsilon^*)P_0}{2\pi\chi_+(k)}$$

$$- \frac{i\gamma k^2(k - i\varepsilon^*)^2\zeta'(0)}{2\pi\chi_+(k)} \qquad (3.65)$$

and recalling that this equation holds along the real k axis.

The term on the left is analytic in the lower half plane while the one on the right is analytic in the upper half plane. Since the two are equal along the real axis we can consider the former to be the analytic continuation of the latter into the lower half plane. In this way we can construct an entire function $E(k)$ as

$$E(k) = \frac{\hat{v}_-(k,a)(k - i\varepsilon^*)^2}{\chi_-(k)} = \frac{- ik^2(k - i\varepsilon^*)^2\hat{P}_+(k,a)}{\chi_+(k)} + \frac{k^2iP_0'}{2\pi\chi_+(k)}$$

$$- \frac{k^2(k - i\varepsilon^*)P_0}{2\pi\chi_+(k)} - \frac{i\gamma k^2(k - i\varepsilon^*)^2\zeta'(0)}{2\pi\chi_+(k)} \qquad (3.66)$$

where $E(k)$ is equal to the "minus" functions for all k in the lower half plane and the "plus" functions for all k in the upper half plane.

Different choices for $E(k)$ will lead to different solutions to the problem. The least singular solution will correspond to the most rapid decay of the Fourier amplitudes (and hence of $E(k)$) as $k \to \infty$. In order for the Fourier transform to exist the Fourier amplitudes must be algebraic at infinity so that $E(k)$ is at most algebraic at infinity. Using this fact and an extended version of the usual Liouville theorem (Noble (p. 6)) we can determine that $E(k)$ must be a polynomial and we write

$$E(k) = \tilde{a} + \tilde{b}k + \ldots + \tilde{q}k^q \qquad (3.67)$$

where q is a finite integer. Combining equations (3.66) and (3.67) we have

$$\hat{V}_{-}(k,a) = \frac{x_{-}(k)}{(k - i\epsilon^*)^2}\left[\tilde{a} + \tilde{b}k + \tilde{c}k^2 + \tilde{d}k^3 + \ldots + \tilde{q}k^q\right] \qquad (3.68)$$

for $\text{Im } k < 0$ and

$$\hat{P}_{+}(k,a) = \frac{P_0'}{2\pi(k - i\epsilon^*)^2} + \frac{iP_0}{2\pi(k - i\epsilon^*)} - \frac{\gamma\zeta'(o)}{2\pi} + \frac{ix_{+}(k)}{k^2(k-i\epsilon^*)^2} \cdot\left[\tilde{a} + \tilde{b}k + \tilde{c}k^2 + \tilde{d}k^3 + \ldots + \tilde{q}k^q.\right] \qquad (3.69)$$

for $\text{Im } k > 0$. It remains to find the coefficients $\tilde{a}$, $\tilde{b}$, etc.

Our choice for the coefficients of the polynomial $E(k)$ will be dictated by the following requirements. These are: (1) that the solution satisfy the boundary condition at upstream infinity (2) that $\hat{P}_{+}$ is analytic in the upper half plane, and (3) that we obtain the least singular solution.

The upstream boundary condition is that the correction to the doubly infinite duct solution (which is what we are constructing here) vanish as $x \to -\infty$ so that we are left with only the imposed forcing (which is given by eq. (3.2)) in the complete solution. The behavior of the pressure as $x \to -\infty$ is determined by the behavior of $\hat{P}_{+}$ as $k \to 0$ (Roos, (1969), p. 151). In order for P to vanish as $x \to -\infty$ the residue of $\hat{P}_{+}$ at $k = 0$ must be zero. This is accomplished by setting $\tilde{a} = \tilde{b} = 0$.

Since we have defined the function $\hat{P}_{+}$ to be analytic in the upper half plane we must retain enogh coefficients, and choose their values, so that the pole at $k = i\epsilon^*$ in equation (3.69) (which lies in the upper half plane) will cancel out. If we expand equation (3.69) near $k = i\epsilon^*$ the singular part becomes

$$\frac{1}{(k - i\epsilon^*)^2}\left[\frac{ix_+(i\epsilon^*)}{(i\epsilon^*)^2}\left(\tilde{c}(i\epsilon^*)^2 + \tilde{d}(i\epsilon^*)^3 + \ldots + \tilde{q}(i\epsilon^*)^q\right) + \frac{p_o'}{2\pi}\right]$$

$$+ \frac{i}{(k - i\epsilon^*)}\left[\left(\frac{x_+'(i\epsilon^*)}{(i\epsilon^*)^2} - \frac{2(i\epsilon^*)x_+(i\epsilon^*)}{(i\epsilon^*)^4}\right)\right.$$

$$\cdot\left(\tilde{c}(i\epsilon^*)^2 + \tilde{d}(i\epsilon^*)^3 + \ldots + \tilde{q}(i\epsilon^*)^q\right)$$

$$\left. + \frac{iP_o}{2\pi} + \frac{ix_+(i\epsilon^*)}{(i\epsilon^*)^2}\left(2\tilde{c}i\epsilon^* + \ldots \tilde{q}q(i\epsilon^*)^{q-1}\right)\right]$$

and the double pole at $k = i\epsilon^*$ will vanish if we choose

$$\tilde{c} = \frac{ip_o'}{2\pi x_+(i\epsilon^*)}\ ,\ \tilde{d} = 0 \tag{3.70}$$

and the overall level of the pressure fluctuations as

$$P_o = \frac{-iP_o' x_+'(i\epsilon^*)}{x_+(i\epsilon^*)} \tag{3.71}$$

the remaining contributions vanishing as $\epsilon^* \to 0$.

The least singular solution (near $x = 0$) will correspond to the one whose Fourier amplitude decays most rapidly as $k \to \infty$. Hence the least singular solution will be obtained by choosing the order of the polynomial $E(k)$ to be as low as possible while accommodating the consistency condition (that $\hat{P}_+$ is analytic in the upper half plane) and the boundary conditions. Since these conditions have already been satisified we will set the remaining coefficients to zero. Then the least singular solution becomes

$$\hat{V}_-(k,a) = \frac{ip_o'}{2\pi x_+(i\epsilon^*)}\ \frac{k^2 x_-(k)}{(k - i\epsilon^*)^2} \tag{3.72}$$

and

$$\hat{P}_+(k,a) = \frac{P_0'}{2\pi(k - i\epsilon^*)^2}\left(1 - \frac{\chi_+(k)}{\chi_+(i\epsilon^*)}\right) + \frac{P_0'\chi_+'(i\epsilon^*)}{2\pi\chi_+(i\epsilon^*)(k - i\epsilon^*)} - \frac{\gamma\,\zeta'(0)}{2\pi} \qquad (3.73)$$

With the boundary values of the solutions thus obtained we can now write down the equations for the flow variables. From equations (3.25), (3.26), and (3.72) we have for the upwash velocity

$$v(x,r) = \frac{iP_0'}{2\pi\chi_+(o)}\int_{-\infty}^{\infty}\chi_-(k)\,\frac{I_1(kr)}{I_1(ka)}\,e^{ikx}\,dk \qquad (3.74)$$

The streamwise velocity can then be determined from the continuity equation (eq. (3.16)) as

$$u(x,r) = \frac{-P_0'}{2\pi\chi_+(o)}\int_{-\infty}^{\infty}\frac{\chi_-(k)}{I_1(ka)}\left[\frac{I_1(kr)}{kr} + I_1'(kr)\right]e^{ikx}\,dk \qquad (3.75)$$

and the pressure from the momentum equation (eq. (3.14))

$$p(x,r) = \frac{-P_0'}{2\pi\chi_+(o)}\int_{-\infty}^{\infty}\frac{\chi_-(k)}{kI_1(ka)}\left[\rho[\omega - kU(r)]\left(\frac{I_1(kr)}{kr} + I_1'(kr)\right) + \rho U'(r)I_1(kr)\right]e^{ikx}\,dk \qquad (3.76)$$

The solutions of equations (3.74) to (3.76) are valid only when Im ω is sufficiently large. The "steady state" solutions for ω real are obtained by analytically continuing these solutions to the real ω axis. From the discussion of the last section we know that if we are in the range of Strouhal number for which instability waves exist and the flow is convectively unstable one of the poles of χ_-, we will call it α, moves from the upper half plane into the lower half plane as

Im $\Omega \to 0$. In the analytic continuation of our solutions then we must deform the integration contour in the k plane (which is originally the real axis) around this pole. We can evaluate the contribution of this pole using the residue theorem. For the upwash velocity this becomes

$$v(x,r) = \frac{iP_0'}{2\pi\chi_+(o)} \int_{-\infty}^{\infty} \chi_-(k) \frac{I_1(kr)}{I_1(ka)} e^{ikx}\, dk$$

$$- \frac{P_0'}{\chi_+(o)} \frac{1}{I_1(\alpha a)} \lim_{k\to\alpha} [(k-\alpha)\chi_-(k)]\, I_1(\alpha r) e^{i\alpha x} \qquad (3.77)$$

Or, making use of the factorization of the kernal function in the second term

$$v(x,r) = \frac{iP_0'}{2\pi\chi_+(o)} \int_{-\infty}^{\infty} \chi_-(k) \frac{I_1(kr)}{I_1(ka)} e^{ikx}\, dk -$$

$$\left[\frac{P_0'}{\chi_+(o)} \frac{\chi_+(\alpha)}{I_1(\alpha a)\chi'(\alpha)}\right] I_1(\alpha r)\, e^{i\alpha x} \qquad (3.78)$$

Equation (3.78) is valid for ω real.

Since α is in the lower half plane when ω is real the second term on the right in equation (3.78) grows exponentially in x. This term represents a Rayleigh instability wave with amplitude $-P_0'\chi_+(\alpha)/I_1(\alpha a)\chi'(\alpha)\chi_+(0)$. We can think of this instability wave as being triggered at the trailing edge of the duct by the external forcing. The ratio of the amplitude of the instability wave to that of the forcing is the so-called coupling coefficient which in this case becomes

$$C_o = \frac{-\chi_+(\alpha)}{\chi_+(o) I_1(\alpha a)\chi'(\alpha)} \qquad (3.79)$$

The magnitude of the coupling coefficient is a measure of the effectiveness of the external disturbance in generating instability waves.

Using the factorization obtained earlier we can compute numerical values for the coupling coefficient over a range of the physical parameters. We do this in the next section.

Before proceeding to the numerical calculation of the coupling coefficient we wish to point out one further feature of this problem.

We could have constructed a particular solution to equations (3.5) to (3.7) and boundary conditions (eqs. (3.3), (3.4) and (3.8)) without regard to causality. This solution would be formally the same as the one constructed here up to equation (3.76). The definitions of the split functions χ_+ and χ_-, however, would be different. In this case the correct half plane for the real roots is determined by allowing ω to have a small positive imaginary part. This small imaginary part will leave the pole $k = \alpha$ in the lower half plane. Hence it will not appear as a pole of $\chi_-(k)$. We can obtain this particular solution from the causal solution (with $\mathrm{Im}\ \omega$ large) by replacing $\chi_{\pm}(k)$ by $(k - \alpha)\chi_{\pm}(k)$. Making this replacement in equation (3.72) (with $\epsilon^* = 0$) gives

$$\hat{V}_-^p(k,a) = \frac{-iP_0'}{2\pi\chi_+(0)\alpha}(k - \alpha)\,\chi_-(k) \qquad (3.80)$$

for the upwash velocity.

From equation (3.33) and (3.64) we can determine that $\chi \sim k^3$ and $\chi_+ \sim k^2$ as $k \to \infty$ for $b \neq 1$. Then by equation (3.34) we must have that $\chi_- \sim k^{-1}$ (for $b \neq 1$). The behavior of v^p near $x = 0$ is determined by the behavior of $\hat{V}_-^p$ as $k \to \infty$ (Roos (1969) p. 151). Inserting the asymptotic behavior of χ_- into equation (3.80) we find that

$$\hat{V}_-^p(k,a) \sim k^0 \text{ as } k \to \infty$$

from which it follows (Lightill) that

$$V^p(x,a) \sim \delta(x) \quad \text{as } x \to 0^+$$

where $\delta(x)$ is the Dirac delta function. Hence v^p has a delta-function like singularity at the trailing edge of the duct. In the next chapter we will construct an eigensolution to equations (2.11) to (2.16) which has the same singularity at the edge as v^p. It will be shown that the difference between the causal solution and the singular particular solution is a constant multiple of this singular eigensolution and that the constant is just equal to that required to cancel the edge singularity in the particular solution and hence satisfy the Kutta condition. These aspects will be discussed in more detail in the next chapter.

3.6 The Coupling Coefficient

For the numerical computations we will return to dimensionless variables. We make the coupling coefficient dimensionless as

$$C = \frac{\rho U_0}{a} C_0 = \frac{-\chi_+(\tilde{\alpha})}{\chi_+(0) I_1(\tilde{\alpha}) \chi'(\tilde{\alpha})} \left(\frac{\rho U_0}{a}\right) \tag{3.81}$$

where χ_+ is given by its infinite product representation (eq. (3.56)), χ is given by equation (3.43) and $'$ now means $d/d\tilde{x}$.

We can rewrite the infinite products in equation (3.56) in a form more convenient for computations by using some results given by Noble (p. 128). Following Noble we compare the asymptotic behavior of the infinite products in equation (3.56) with that of

$$J(\tilde{x}) = \prod_{n=1}^{\infty} \left(1 + \frac{\tilde{x}}{a_1 n + b_1}\right) e^{-\tilde{x}/a_1 n} = e^{-c\tilde{x}/a_1} \frac{\Gamma\left(\frac{b_1}{a_1} + 1\right)}{\Gamma\left(\frac{\tilde{x}}{a_1} + \frac{b_1}{a_1} + 1\right)} \tag{3.82}$$

where a_1 and b_1 are the coefficients in the asymptotic form of the roots, and c is Euler's constant ($c = 0.5772 \ldots$).

If we divide the infinite products in equation (3.56) by the infinite product representation of J and insert the values for a_1 and b_1 we can write

$$\frac{x_+^N(\tilde{x})}{J^N(\tilde{x})} = e^{\tilde{x}\sum_{n=1}^{\infty}(1/i\pi n - 1/\tilde{\zeta}_n)} \prod_{n=1}^{\infty}\left[\frac{i\pi n + \frac{i\pi}{4}(1-4\ell)}{\tilde{\zeta}_n}\right] \cdot \prod_{n=1}^{\infty}\left[1 + \frac{\tilde{\zeta}_n - i\pi n - \frac{i\pi}{4}(1-4\ell)}{i\pi n + \frac{i\pi}{4}(1-4\ell) + \tilde{x}}\right] \tag{3.83}$$

and

$$\frac{x_+^D(\tilde{x})}{J^D(\tilde{x})} = e^{\tilde{x}\sum_{n=1}^{\infty}(1/i\pi n - 1/\tilde{\beta}_n)} \prod_{n=1}^{\infty}\left[\frac{i\pi n + \frac{i\pi}{4}}{\tilde{\beta}_n}\right] \cdot \prod_{n=1}^{\infty}\left[1 + \frac{\tilde{\beta}_n - i\pi n - \frac{i\pi}{4}}{i\pi n + \frac{i\pi}{4} + \tilde{x}}\right] \tag{3.84}$$

where the superscripts N and D are used to distinguish between the infinite products in the numerator and denominator, respectively.

From the gamma function representation of J we have

$$J^N(\tilde{x}) = e^{-c\tilde{x}/i\pi} \frac{\Gamma\left(\frac{5}{4} - \ell\right)}{\Gamma\left(\frac{\tilde{x}}{i\pi} + \frac{5}{4} - \ell\right)} \tag{3.85}$$

$$J^D(\tilde{x}) = e^{-c\tilde{x}/i\pi} \frac{\Gamma\left(\frac{5}{4}\right)}{\Gamma\left(\frac{\tilde{x}}{i\pi} + \frac{5}{4}\right)} \tag{3.86}$$

From the functional equation for the gamma function

$$\Gamma\left(\frac{5}{4}\right) = \left(\frac{5}{4} - 1\right) \ldots \left(\frac{5}{4} - \ell\right) \Gamma\left(\frac{5}{4} - \ell\right) \tag{3.87}$$

and

$$\Gamma\left(\frac{\tilde{x}}{i\pi} + \frac{5}{4}\right) = \left(\frac{\tilde{x}}{i\pi} + \frac{5}{4} - 1\right) \cdots \left(\frac{\tilde{x}}{i\pi} + \frac{5}{4} - \ell\right) \Gamma\left(\frac{\tilde{x}}{i\pi} + \frac{5}{4} - \ell\right) \tag{3.88}$$

Combining equations (3.56) (3.63) and (3.82) to (3.88) we can write a new expression of χ_+ as

$$\chi_+(\tilde{x}) = \frac{\prod_{n=1}^{\infty}\left(\frac{in\pi + \frac{i\pi}{4}(1 - 4\ell)}{\tilde{\zeta}_n}\right)}{\prod_{n=1}^{\infty}\left(\frac{in\pi + \frac{i\pi}{4}}{\tilde{\beta}_n}\right)} \cdot \frac{\left(\frac{\tilde{x}}{i\pi} + \frac{5}{4} - 1\right) \cdots \left(\frac{\tilde{x}}{i\pi} + \frac{5}{4} - \ell\right)}{\left(\frac{5}{4} - 1\right) \cdots \left(\frac{5}{4} - \ell\right)}$$

$$\cdot \frac{\prod_{n=1}^{\infty}\left[1 + \frac{\tilde{\zeta}_n - i\pi n - \frac{i\pi}{4}(1 - 4\ell)}{i\pi n + \frac{i\pi}{4}(1 - 4\ell) + \tilde{x}}\right]}{\prod_{n=1}^{\infty}\left[1 + \frac{\tilde{\beta}_n - i\pi n - \frac{i\pi}{4}}{i\pi n + \frac{i\pi}{4} + \tilde{x}}\right]} \tag{3.89}$$

The roots $\tilde{\zeta}_n$ and $\tilde{\beta}_n$ approach their asymptotic values fairly quickly. Expressing the terms in the infinite products so that they occur as differences between the roots and their asymptotic values reduces the number of arithmetic operations needed before the products can be considered converged. Not only is the computation time reduced by this procedure but the error due to roundoff which would accumulate after many operations is minimized.

We can use equations (3.44) to (3.46) to write $\chi'(\tilde{\alpha})$ as

$$\chi'(\tilde{\alpha}) = \frac{1}{\left[\Omega - \tilde{\alpha}(1 - b)\right]} F_1'(\tilde{\alpha}) \left[\frac{\tilde{\alpha}}{I_1(\tilde{\alpha})}\right] \left(\frac{\rho U_0}{a}\right) \tag{3.90}$$

by noting that $F_1(\tilde{\alpha}) = 0$.

From equation (3.56) we see that $\chi_+(o) = 1$.

Combining equations (3.81), (3.89), and (3.90) along with the fact that $\ell = 2$ to write the final computational formula for the coupling coefficient as

$$C = \frac{16}{3}\frac{[\Omega - \tilde{\alpha}(1-b)]}{F_1'(\tilde{\alpha})\tilde{\alpha}}\left(\frac{\tilde{\alpha}}{i\pi}+\frac{1}{4}\right)\left(\frac{\tilde{\alpha}}{i\pi}-\frac{3}{4}\right)\cdot\frac{\prod_{n=1}^{\infty}\left[\frac{in\pi - \frac{7i\pi}{4}}{\tilde{\zeta}_n}\right]}{\prod_{n=1}^{\infty}\left[\frac{in\pi + \frac{i\pi}{4}}{\tilde{\beta}_n}\right]}$$

$$\cdot\frac{\prod_{n=1}^{\infty}\left[1+\frac{\tilde{\zeta}_n - i\pi n + \frac{7i\pi}{4}}{i\pi n - \frac{7i\pi}{4}+\tilde{\alpha}}\right]}{\prod_{n=1}^{\infty}\left[1+\frac{\tilde{\beta}_n - i\pi n - \frac{i\pi}{4}}{i\pi n + \frac{i\pi}{4}+\tilde{\alpha}}\right]} \qquad (3.91)$$

We now give the results of the numerical evaluation of the coupling coefficient using equation (3.91).

3.7 Numerical Results

Numerical values for the magnitude of the coupling coefficient were computed for the mean velocity profiles considered in section 3.4.3 and a number of Weber numbers over the range of Strouhal numbers for which spatially growing waves were found to exist (see section 3.4.3).

Figures 3.21 to 3.23 show the results of the computations. Each curve in these plots show the variation of the magnitude of the coupling coefficient with Strouhal number for a fixed Weber number.

For the plug profile (fig. 3.21) $|C|$ is nearly independent of β^2 over the range shown while for the other mean profiles (figs. 3.21 and 3.23) $|C|$ increases with increasing Weber number.

According to these results, for a given profile and Weber number, the greatest coupling generally occurs for smaller Strouhal numbers although there are curves ($b = 0.4$, $\beta^2 = 10$ most notably) for which $|C|$ reaches a minimum and then begins to increase as the cutoff Strouhal number is approached. By superposing these figures we can determine the effect of the mean velocity profile on $|C|$. When this is done it can be seen that, for fixed Strouhal and Weber numbers, the magnitude of the coupling coefficient increases with increasing b. This result indicates that a greater coupling could be achieved in practice if a longer nozzle were used since then the mean profile would be more fully developed. Along with this increase of the coupling coefficient however comes a decrease in the growth rate of the instability wave (see section 3.4.3).

CHAPTER 4

THE EIGENSOLUTION

4.1 Introduction

In the previous chapter, in addition to obtaining a causal solution, we obtained a noncausal, singular particular solution to the boundary value problem in section 3.6. We will show that the singularity in this particular solution can be removed by adding the correct multiple of an eigensolution which has the same order of singularity. The resulting nonsingular solution is said to satisfy the Kutta condition. It remains to be determined however whether or not the solution obtained using the Kutta condition is causal.

We will construct the necessary eigensolution in this chapter. Once this has been done the eigensolution will be combined with the particular solution (eq. (3.80)) in such a way as to eliminate the singularity. The nonsingular solution thus obtained will then be compared with the causal solution obtained in Chapter 3. As in the previous chapter we construct the eigensolution by superposition.

First we consider the flow of a doubly infinite jet of fluid in the absence of any duct. That is, we find a solution to equations (2.11) to (2.13) subject to free surface boundary conditions for all x, $-\infty < x < \infty$. Since this solution (which is a Rayleigh instability wave) will not satisfy the boundary condition on the solid duct wall, a solution is constructed which cancels the normal velocity on the boundary for $x < 0$. The sum of these two solutions then is the desired eigensolution.

4.2 Doubly Infinite Jet

In this section we seek solutions to equations (2.11) to (2.13) subject to the free surface boundary conditions (eqs. (2.15) and (2.16)) for all x, $-\infty < x < \infty$. We look for solutions of the form

$$(u^I, v^I, p^I, \zeta^I) = (\hat{u}^I(r), \hat{v}^I(r), \hat{p}^I(r)), \hat{\zeta}^I) e^{i\alpha(x-ct)} \tag{4.1}$$

where $\alpha c = \omega$ with α and c complex. Substituting equation (4.1) into the equations of motion we obtain the following equations for the "^" functions

$$\rho i(U(r) - c)\, \hat{u}^I(r) + \rho \hat{v}^I(r) \frac{dU(r)}{dr} = i\alpha \hat{p}^I(r) \tag{4.2}$$

$$\rho i\alpha(U(r) - c)\, \hat{v}^I(r) = -\hat{p}^{I'}(r) \tag{4.3}$$

and

$$i\alpha \hat{u}^I(r) + \frac{1}{r} \frac{d}{dr} [r\hat{v}^I(r)] = 0 \tag{4.4}$$

These equations are formally identical to equations (3.14) to (3.16) of Chapter 3 (in this case the functions are the normal mode solutions whereas before they were Fourier transforms). They can be manipulated in the same way to obtain the Rayleigh equation for $\hat{v}^I$ as

$$(U(r) - c)\hat{v}^{I''}(r) + \frac{(U(r) - c)}{r} \hat{v}^{I'}(r) - r \frac{d}{dr}\left[\frac{U'(r)}{r}\right] + (U(r) - c)\left(\alpha^2 + \frac{1}{r^2}\right) \hat{v}^I(r) = 0 \tag{4.5}$$

Substituting the family of velocity profiles we are considering

$$U(r) = U_o\left(1 - b \frac{r^2}{a^2}\right) \tag{4.6}$$

we can again arrive at the modified Bessel equation for $\hat{v}^I$

$$\hat{v}^{I''}(r) + \frac{1}{r} \hat{v}^{I'}(r) - \left(\alpha^2 + \frac{1}{r^2}\right) \hat{v}^I(r) = 0 \tag{4.7}$$

After applying a boundedness condition on the solution at $r = 0$ we obtain

$$\hat{v}^I(r) = AI_1(\alpha r) \tag{4.8}$$

where A is an arbitrary constant.

The boundary conditions (eqs. (2.15) and (2.16)) determine the values of α for which nontrivial solutions exist, that is the eigenvalues. Using equation (4.1) in equations (2.15) and (2.16) we obtain

$$\hat{v}^I(a) = i\alpha\, \hat{\zeta}^I(a)(U(a) - c) \tag{4.9}$$

and

$$\hat{p}^I(a) = \gamma\, \hat{\zeta}^I(a) \left(\alpha^2 - \frac{1}{a^2}\right) \tag{4.10}$$

Eliminating $\hat{\zeta}^I(a)$ from these two equations we can write

$$\frac{\hat{v}^I(a)}{i\alpha(U(a) - c)} = \frac{\hat{p}^I(a)}{\gamma\left(\alpha^2 - \frac{1}{a^2}\right)} \tag{4.11}$$

Another relation between $\hat{v}^I(a)$ and $\hat{p}^I(a)$ can be obtained by eliminating $\hat{u}^I$ between equations (4.2) and (4.4) and evaluating at $r = a$. Upon substituting for the mean flow profile (eq. (4.6)) this relation becomes

$$\hat{p}^I(a) = \frac{-\rho i}{\alpha} \left[\hat{v}^I(a)\left(\frac{2U_0 b}{a} + \frac{U_0(1 - b) - c}{a}\right) + (U_0(1 - b) - c)\, \hat{v}^{I'}(a)\right] \tag{4.12}$$

We can now combine equations (4.11) and (4.12) along with the solution (eq. (4.8)) to obtain the eigenvalue relation

$$\frac{I_1(\alpha a)}{[\omega - U_0(1 - b)\alpha]} = \frac{\rho a^3}{\gamma} \frac{1}{\alpha a(\alpha^2 a^2 - 1)} \times \left[\frac{\omega - U_0(b + 1)\alpha}{\alpha a} I_1(\alpha a) + [\omega - U_0(1 - b)\alpha]\, I_1'(\alpha a)\right] \tag{4.13}$$

For the case $b = 0$ this reduces to

$$\frac{I_1(\alpha a)}{[\omega - U_0\alpha]} = \frac{\rho a^3}{\gamma} \frac{1}{\alpha a(\alpha^2 a^2 - 1)} \left[\frac{\omega - U_0\alpha}{\alpha a} I_1(\alpha a) + (\omega - U_0\alpha)\, I_1'(\alpha a)\right] \tag{4.14}$$

which agrees with the result obtained by Keller et al. (1973).

Equations (4.8) and (4.13) give the eigenfunctions and eigenvalues of the normal mode solution for the doubly infinite jet. We will now construct a solution which corrects the normal mode solution for the presence of the semi-infinite duct.

4.3 Semi-infinite Jet

The solution constructed in section 4.2 has a nonzero normal velocity on the boundary for $x < 0$. To correct for the existence of the rigid duct walls we must superpose on this solution one which cancels the normal velocity on the boundary for $x < 0$.

Specifically, we seek functions $\bar{u}$, $\bar{v}$, $\bar{p}$ and $\bar{\zeta}$ which satisfy equations (2.11) to (2.13), boundary conditions (eqs. (2.15) and (2.16)) for $x > 0$ and the following boundary conditions for $x < 0$

$$\bar{v}(x,a,t) = -AI_1(\alpha a)\, e^{i(\alpha x-\omega t)} \tag{4.18}$$

The boundary condition eq. (4.18) ensures that the normal velocity at $r = a$ is equal and opposite to that in the solution of section 4.2. Applying the unilateral Fourier transform (eq. (3.11)) to the boundary condition (eq. (4.18)) we get

$$\hat{V}_+(k,a) = \frac{iAI_1(\alpha a)}{2\pi(\alpha - k)} \tag{4.19}$$

As in Chapter 3 we will assume time harmonic solutions which can be Fourier transformed in x and use the Wiener-Hopf technique.

The same manipulations leading to the Wiener-Hopf equation in Chapter 3 can be performed here as well. The only difference being in the inhomogeneous terms in the Weiner-Hopf equation (due to the different boundary conditions for the two problems). Without repeating the algebra here we simply write down the Wiener-Hopf equation for this problem as

$$\chi(k)\,\hat{V}_-(k,a) + ik^2\hat{P}_+ = -\left[\chi(k) + \frac{\gamma k^2(k^2 - 1/a^2)}{[\omega - kU(a)]}\right]\cdot \frac{iAI_1(\alpha a)}{2\pi(\alpha - k)} - \frac{i\gamma k^2\zeta'(0)}{2\pi} \qquad (4.20)$$

In constructing the (singular) eigensolution, as in the particular solution, the frequency ω is allowed to have a small positive imaginary part. The factorization of $\chi(k)$ when $\mathrm{Im}\,\omega$ is small is related to the factorization when $\mathrm{Im}\,\omega$ is large by

$$\tilde{\chi}_{\pm}(k) = \chi_{\pm}(k)\,(k - \alpha) \qquad (4.21)$$

where $\chi_{\pm}$ are the split functions obtained in Chapter 3 with $\mathrm{Im}\,\omega >> 1$. Using the functions $\tilde{\chi}_{\pm}$ here we can rewrite equation (4.19) as

$$\frac{\hat{V}_-(k,a)}{\tilde{\chi}_-(k)} + \frac{ik^2\hat{P}_+(k,a)}{\tilde{\chi}_+(k)} = -\left[\frac{1}{\tilde{\chi}_-(k)} + \frac{\gamma k^2(k^2 - 1/a^2)}{\tilde{\chi}_+(k)[\omega - kU(a)]}\right]\cdot \frac{iAI_1(\alpha a)}{2\pi\,(\alpha - k)} - \frac{i\gamma k^2\zeta'(0)}{2\pi\tilde{\chi}_+(k)} \qquad (4.22)$$

The last term on the right hand side of equation (4.22) is already a "plus" function. The remaining inhomogeneous terms must be factored by subtracting out poles. For this purpose we define

$$G(k) = \frac{-iAI_1(\alpha a)}{2\pi}\left[\frac{1}{\tilde{\chi}_-(k)(\alpha - k)} + \frac{\gamma k^2(k^2 - 1/a^2)}{\tilde{\chi}_+(k)[\omega - kU(a)](\alpha - k)}\right] \qquad (4.23)$$

and construct functions G_+ and G_- so that

$$G(k) = (G_+(k) + G_-(k)) \qquad (4.24)$$

where G_+ is analytic in the upper half k plane and G_- is analytic in the lower half plane. By inspecting equation (4.23) we can see that the desired functions are

$$G_+(k) = \frac{-iAI_1(\alpha a)}{2\pi(\alpha - k)\tilde{\chi}_-(\alpha)} - \frac{iAI_1(\alpha a)\ \gamma k^2(k^2 - 1/a^2)}{(\alpha - k)[\omega - kU(a)]\tilde{\chi}_+(k)2\pi} +$$

$$+ \frac{\gamma\left(\frac{\omega}{U(a)}\right)^2\left(\left(\frac{\omega}{U(a)}\right)^2 - 1/a^2\right)iAI_1(\alpha a)}{\left(\alpha - \frac{\omega}{U(a)}\right)\tilde{\chi}_+\left(\frac{\omega}{U(a)}\right)[\omega - kU(a)]2\pi} \qquad (4.25)$$

$$G_-(k) = \frac{-iAI_1(\alpha a)}{2\pi(\alpha - k)\tilde{\chi}_-(k)} + \frac{iAI_1(\alpha a)}{2\pi(\alpha - k)\tilde{\chi}_-(\alpha)} -$$

$$- \frac{\gamma\left(\frac{\omega}{U(a)}\right)^2\left(\left(\frac{\omega}{U(a)}\right)^2 - 1/a^2\right)iAI_1(\alpha a)}{\left(\alpha - \frac{\omega}{U(a)}\right)\tilde{\chi}_+\left(\frac{\omega}{U(a)}\right)[\omega - kU(a)]2\pi} \qquad (4.26)$$

Substituting equations (4.25) and (4.26) into equation (4.24) and rearranging we get

$$\frac{\hat{V}_-(k,a)}{\tilde{\chi}_-(k)} + \frac{iAI_1(\alpha a)}{2\pi(\alpha - k)\tilde{\chi}_-(k)} - \frac{iAI_1(\alpha a)}{2\pi(\alpha - k)\tilde{\chi}_-(\alpha)} +$$

$$+ \frac{\gamma\left(\frac{\omega}{U(a)}\right)^2\left(\left(\frac{\omega}{U(a)}\right)^2 - 1/a^2\right)iAI_1(\alpha a)}{\left(\alpha - \frac{\omega}{U(a)}\right)\tilde{\chi}_+\left(\frac{\omega}{U(a)}\right)[\omega - kU(a)]} = \frac{-ik^2\hat{P}_+(k,a)}{\tilde{\chi}_+(k)} + \frac{-iAI_1(\alpha a)}{2\pi(\alpha - k)\tilde{\chi}_-(\alpha)}$$

$$- \frac{\gamma k^2(k^2 - 1/a^2)\ iAI_1(\alpha a)}{(\alpha - k)[\omega - kU(a)]\tilde{\chi}_+(k)2\pi} + \frac{\gamma\left(\frac{\omega}{U(a)}\right)^2\left(\left(\frac{\omega}{U(a)}\right)^2 - 1/a^2\right)iAI_1(\alpha a)}{\left(\alpha - \frac{\omega}{U(a)}\right)\tilde{\chi}_+\left(\frac{\omega}{U(a)}\right)[\omega - kU(a)]2\pi}$$

$$- \frac{i\gamma k^2\zeta'(o)}{2\pi\tilde{\chi}_+(k)} = \tilde{E}(k) \qquad (4.27)$$

where $E(k)$ is an entire function which, by the same arguments used in Chapter 3, is a polynomial.

Replacing $E(k)$ with a polynomial and returning to the split functions $\chi_{\pm}$ by equation (4.21) we can write the solution to the Wiener-Hopf equation as

$$\hat{V}_{-}(k,a) = (k-\alpha)\chi_{-}(k)\left[\tilde{a}' + \tilde{b}'k + \ldots + \tilde{q}'k^{q}\right] - \frac{iAI_1(\alpha a)}{2\pi(\alpha - k)}$$

$$- \frac{iAI_1(\alpha a)\chi'(\alpha)\chi_{-}(k)}{2\pi\chi_{+}(\alpha)} + \frac{iAI_1(\alpha a)\gamma\left(\frac{\omega}{U(a)}\right)^2\left(\left(\frac{\omega}{U(a)}\right)^2 - 1/a^2\right)}{\chi_{+}\left(\frac{\omega}{U(a)}\right)\left(\alpha - \frac{\omega}{U(a)}\right)^2 2\pi} \frac{(k-\alpha)\chi_{-}(k)}{[\omega - kU(a)]}$$

(4.28)

and

$$\hat{P}_{+}(k,a) = \frac{i(k-\alpha)\chi_{+}(k)}{k^2}\left[\tilde{a}' + \tilde{b}'k + \ldots + \tilde{q}'k^{q}\right] - \frac{AI_1(\alpha a)\chi'(\alpha)\chi_{+}(k)}{2\pi\chi_{+}(\alpha)k^2}$$

$$- \frac{AI_1(\alpha a)\gamma k^2(k^2 - 1/a^2)}{2\pi k^2(\alpha - k)[\omega - kU(a)]} - \frac{AI_1(\alpha a)\gamma\left(\frac{\omega}{U(a)}\right)^2\left(\left(\frac{\omega}{U(a)}\right)^2 - 1/a^2\right)(k-\alpha)\chi_{+}(k)}{\chi_{+}\left(\frac{\omega}{U(a)}\right)\left(\alpha - \frac{\omega}{U(a)}\right)^2 2\pi[\omega - kU(a)]k^2}$$

$$- \frac{\gamma\zeta'(0)}{2\pi} \qquad (4.29)$$

As in Chapter 3 we will choose the coefficients $\tilde{a}'$, $\tilde{b}'$, etc. so that (1) $\hat{P}_{+}$ is analytic in the upper half plane, (2) there are no poles at $k = 0$, and (3) we obtain the least singular solution near $x = 0$.

The singular part of $\hat{P}_{+}$ near $k = 0$ can be found to be

$$\frac{1}{k^2}\left[-i\alpha\chi_{+}(0)\tilde{a}' - \frac{AI_1(\alpha a)\chi'(\alpha)\chi_{+}(0)}{2\pi\chi_{+}(\alpha)} + \frac{AC\alpha\chi_{+}(0)}{i\omega}\right] + \frac{1}{k}\left[-i\alpha\chi_{+}(0)\tilde{b}' + \right.$$

$$+ i\tilde{a}'\left(-\alpha\chi_{+}'(0) + \chi_{+}(0)\right) - \frac{AI_1(\alpha a)\chi'(\alpha)\chi_{+}'(0)}{2\pi\chi_{+}(\alpha)}$$

$$\left. - \frac{AC}{\omega^2 i}\left(\omega(-\alpha\chi_{+}'(0) + \chi_{+}(0)) - \alpha\chi_{+}(0)U(a)\right)\right] \qquad (4.30)$$

In order to eliminate the pole at $k = 0$ we must set

$$\tilde{a}' = \frac{-i}{\alpha}\left[\frac{-AI_1(\alpha a)\chi'(\alpha)}{2\pi\chi_+(\alpha)} + \frac{AC\alpha}{i\omega}\right] \tag{4.31}$$

and

$$\tilde{b}' = \frac{-i}{\alpha}\left[i\tilde{a}' - \frac{AC}{i\omega} + \frac{AC\alpha U(a)}{i\omega^2}\right] \tag{4.32}$$

where

$$C = \frac{iI_1(\alpha a)\gamma\left(\frac{\omega}{U(a)}\right)^2\left(\left(\frac{\omega}{U(a)}\right)^2 - 1/a^2\right)}{2\pi\chi_+\left(\frac{\omega}{U(a)}\right)\left(\alpha - \frac{\omega}{U(a)}\right)^2} \tag{4.33}$$

This choice for $\tilde{a}'$ and $\tilde{b}'$ ensures that the pressure decays at upstream infinity and that $\hat{p}_+$ is analytic in the upper half plane. With these conditions satisfied then we can obtain the least singular solution by setting the remaining coefficients equal to zero. Hence, we can rewrite equations (4.28) and (4.29) as

$$\hat{V}_-(k,a) = (k - \alpha)\chi_-(k)(\tilde{a}' + \tilde{b}'k) - \frac{iAI_1(\alpha a)}{2\pi(\alpha - k)} - \frac{iAI_1(\alpha a)\chi'(\alpha)\chi_-(k)}{2\pi\chi_+(\alpha)} + \frac{AC(k - \alpha)\chi_-(k)}{[\omega - kU(a)]} \tag{4.34}$$

and

$$P_+(k,a) = \frac{i(k - \alpha)\chi_+(k)}{k^2}\left(\tilde{a}' + \tilde{b}'k\right) - \frac{AI_1(\alpha a)\chi'(\alpha)\chi_+(k)}{2\pi\chi_+(\alpha)k^2} - \frac{AI_1(\alpha a)\gamma k^2(k^2 - 1/a^2)}{2\pi k^2(\alpha - k)[\omega - kU(a)]} + \frac{+iAC(k - \alpha)\chi_+(k)}{[\omega - kU(a)]k^2} - \frac{\gamma\zeta'(0)}{2\pi} \tag{4.35}$$

The purpose of constructing an eigensolution to the problem was to use it to eliminate the edge singularity in the noncausal particular solution (eq. (3.80)). However by examining equations (3.80) and (4.34) we see that the least singular eigensolution we were able to construct

(consistent with the boundary conditions at upstream infinity) has a higher order singularity than the particular solution equation (3.80). If we try to remove the singularity in the particular solution by adding this eignsolution we will still be left with a singularity at the edge of the duct and hence the resulting solution will still not satisfy the Kutta condition (in fact it will not even exist in the usual sense). Evidently another eignsolution must be added to relieve this singularity.

4.4 The Kutta Condition

The difference between the causal and noncausal particular solution must satisy the differential equations (2.11) to (2.13) subjet to homogeneous boundary conditions, that is it must be an eigensolution. From equations (3.17), (3.78), and (3.80) we can find this eigensolution for the upwash velocity to be

$$v^e(x,a) = \int_{-\infty}^{\infty} \frac{iP_0' \chi_-(k)}{2\pi\chi_+(0)} \left[1 + \frac{(k-\alpha)}{\alpha}\right] e^{ikx} dk - \frac{+P_0' \chi_+(\alpha)}{\chi_+(0) I_1(\alpha a) \chi'(\alpha)} I_1(\alpha a) e^{i\alpha x} \tag{4.36}$$

If we rearrange equation (4.34) we can write it as

$$\hat{v}(k,a) = \left\{ (k-\alpha)\chi_-(k) \left[\frac{-iAI_1(\alpha a)\chi'(\alpha)}{2\pi\alpha\chi_+(\alpha)} - \frac{AC}{\omega} + \frac{AC}{\omega} \right] - \frac{iAI_1(\alpha a)}{2\pi(\alpha - k)} \right.$$

$$\left. - \frac{iAI_1(\alpha a)\chi'(\alpha)\chi_-(k)}{2\pi\chi_+(\alpha)} \right\} + \left\{ (k-\alpha)\chi_-(k) \left[-\frac{AC}{\omega} + \tilde{b}'k \right] + \frac{AC(k-\alpha)\chi_-(k)}{[\omega - kU(a)]} \right\} \tag{4.37}$$

Combining equations (4.8), (4.19), and (4.37), we can write the complete eigensolution we have constructed as

$$v^E(x,a) = \int_{-\infty}^{\infty} \frac{-iAI_1(\alpha a)\chi'(\alpha)}{2\pi\chi_+(\alpha)} \chi_-(k)\left(\frac{(k-\alpha)}{\alpha} + 1\right) e^{ikx}dk + AI_1(\alpha a)\, e^{i\alpha x}$$

$$+ \int_{-\infty}^{\infty} \left\{(k-\alpha)\chi_-(k)\left[-\frac{AC}{\omega} + \tilde{b}'k\right] + \frac{AC(k-\alpha)\chi_-(k)}{[\omega - kU(a)]}\right\} e^{ikx}dk \qquad (4.38)$$

The first two terms on the right in equation (4.38) are equal, to within a multiplicative constant, to the eigensolution (4.36). The remaining term then must by itself be an eigensolution with the same level of singularity as the eigensolution we constructed in the last section.

We write this eigensolution as

$$v^E(x,a) = \int_{-\infty}^{\infty} (k-\alpha)\,\chi_-(k) - \left[\frac{AC}{\omega} + \tilde{b}'k + \frac{AC}{[\omega - kU(a)]}\right] e^{ikx}dk \qquad (4.39)$$

If we added the eigensolution (4.38) and subtracted (4.39) from the noncausal particular solution we could eliminate all the singularities by choosing the constant A correctly and we would of course arrive back at the causal solution.

Naturally we cannot conclude from the discussion of this section that all solutions which satisfy the edge condition are causal. However, with the procedure used here, we were not able to construct any noncausal solutions which satisfied the edge condition.

4.5 The Effect of the Mean Flow Profile on the roots of the Dispersion Equation

Before closing this chapter we explore the effect of the mean flow profile on the roots of the dispersion equation (eq. (4.13)). The inclusion of the parameter b allows us to trace the evolution of these roots as the mean profile goes from plug flow (b = 0) to a Hagen-Poiseville parabolic profile (b = 1).

For the numerical computations we write equation (4.13) in dimensionless form as

$$[\Omega - \tilde{x}(1 - b)]^2\left[1 + \frac{\tilde{x}I_1'(\tilde{x})}{I_1(\tilde{x})}\right] - 2\tilde{x}[\Omega - \tilde{x}(1 - b)]b + \frac{\tilde{x}^2(1 - \tilde{x}^2)}{\beta^2} = 0 \qquad (4.40)$$

Roots corresponding to the lowest instability modes were computed over a range of Strouhal and Weber numbers. Figures 4.1 to 4.5 show the development of these roots as b goes from 0 to 1. In these figures Im $\tilde{x}$ corresponds to the growth rate of a disturbance with wavenumber Re $\tilde{x}$.

CHAPTER 5

DISCUSSION AND SUMMARY

We have examined the possibility of exciting capillary instabilities in a circular liquid jet by forcing the flow from within the nozzle. This is the so-called receptivity problem. A time harmonic axial pressure gradient was imposed on the steady, parallel flow of a jet emanating from a semi-infinite circular duct.

Using a method developed in the study of plasma instabilities we were able to construct a time harmonic causal solution to the forced problem over certain ranges of the physical parameters. In order for this time harmonic solution to be causal it must contain a term which grows exponentially in the downstream direction, in other words an instability wave. Hence causality provides a mechanism by which externally imposed disturbances can couple to instability waves. In addition, causality uniquely specifies the amplitude of the instability wave relative to that of the forcing and hence the "coupling coefficient" is determined. This "coupling coefficient" is a measure of the effectiveness of the disturbance in generating instability waves. The analysis of Chapter 3 yielded a formula for the coupling coefficient from which numerical values were computed for different combinations of mean profile, Weber number, and Strouhal number.

In the process of constructing a causal solution we found a range of Weber numbers (in particular Weber numbers less than around 5) for which a time harmonic "steady-state" solution does not exist. For these Weber numbers a disturbance will grow exponentially in time at every point in space so that the concept of spatially growing waves is no longer applicable. In this case the flow is said to be absolutely unstable. Since we are interested in generating spatially growing waves

we have restricted our attention to the range of Weber number for which a "steady-state" solution exists and have not further pursued the case of absolute instability.

In addition to the casual solution obtained by the method described in the appendix a noncausal solution to the forced problem was found. The noncausal solution had a delta function singularity at the trailing edge of the duct. In order to obtain a solution which satisfies the Kutta condition a constant multiple of an eigensolution, with the same level edge singularity can be added to the forced solution so that the singularity is cancelled out.

In Chapter 4 we constructed an eigensolution to the equations and boundary conditions set down in Chapter 2. However, the least singular eigensolution we were able to construct contained a higher order edge singularity than the noncausal particular solution. Hence the sum of the two still would not satisfy the Kutta condition. We were able to eliminate all the singularities by appealing back to the solutions of Chapter 3 but this inevitably led us back to the causal solution in order satisfy the edge condition. That is to say we were not able to construct any noncausal solution which satisfied the edge conditions.

In constructing the eigensolution in Chapter 4 we derived the dispersion relation for the stability problem of the doubly infinite jet for the family of mean profiles given by eq. (3.21). The lowest order root in the fourth quadrant of the complex wave number plane was computed for this family of profiles over a range of Weber and Strouhal numbers extending the results of Keller et al. (1973) who computed this root for the plug flow profile ($b = 0$).

5.2 Prospects for Further Research

The discovery that the liquid jet can support absolute instabilities was an unexpected result which deserves more attention. By a detailed numerical investigation of the dispersion relation it would be possible to pin down, for each mean profile, the range of Weber number for which the absolute instabilities arise. It may even be possible to determine this range analytically for the plug flow profile.

The effects of viscosity on the coupling coefficient and growth rates of the instability waves have not been considered in this work and would make an interesting extension of the results obtained here.

APPENDIX A

A.1 Introduction

In this appendix we will outline some of the theory behind the criteria used in the main body of this work to ensure that causality is satisfied and identify absolute instabilities. The mathematics was worked out originally for the study of plasma instabilities. We have used the results as derived by Briggs (1964) and Bers (1972) and reference will be made to them for detailed proofs.

The method for obtaining a causal solution is based on the examination of an initial value problem where the forcing is "turned on" at some initial time. The "steady state" solution will be the long time behavior of the solution to this initial value problem provided that the flow is not absolutely unstable.

A description of the method and a discussion of the issue of absolute instability is given in the following two sections. Since we have a specific example in the present problem we will use it to illustrate the ideas.

A.2 Method of Solution

We consider an initial value problem. At time $t = 0$ the flow in the semi-infinite jet is subjected to a pulsating axial pressure gradient. The response of the flow to this forcing in space and time can be determined by an inverse transform of the Greens function for this problem in the frequency and wave number planes as

$$g(x,t) = \int_L \int_F G(\omega,k)\, e^{ikx}\, e^{i\omega t}\, dk\, d\omega \qquad (A1)$$

or as a function of frequency as

$$g(x,\omega) = \int_F G(\omega,k)\, e^{ikx}\, dk \qquad (A2)$$

This Greens' function will have poles at the zeros of the dispersion relation in the k and ω planes. The inversion contour in the frequency plane must be a line such that no zeros of the dispersion relation (complex ω for real k) exist above it, since only then will the condition of causality be satisfied (for $t < 0$ the integral is evaluated by closing the contour in the upper half ω plane). The integration contours in the k and ω planes are shown in figure A.1. Therefore, we need to obtain the solution in the frequency plane along this contour L, that is for the frequency having a sufficiently large positive imaginary part.

We are interested in the asymptotic response of the flow a long time after the forcing was initiated. The asymptotic response can be obtained by moving the contour in the ω plane as close as possible to the real axis (since, in the absence of absolute instabilities the behavior of the solution for large t is determined by the pole of g nearest the real axis in the ω plane). If we can move the contour all the way to the real axis, that is if we can analytically continue g to the real axis, then the long time response will be due to a pole on the real axis which corresponds to the frequency of the forcing. In this case then a time harmonic, "steady state" solution exists.

Now the poles in the k plane are related to ω through the dispersion relation, say $\Delta(k,\omega) = 0$. As we let ω approach the real ω axis it may happen that certain poles in the k plane cross the real k axis (in fact, if instability waves are to be generated by the forcing this must happen). If this happened $g(x,\omega)$ would not be analytic unless the contour in the k plane is deformed so as to continue to include (or exclude) any poles which might be inclined to cross the real axis as $\text{Im}\ \omega \to 0$. This is illustrated in figure A.2.

The spatial response of the flow is obtained by closing the integration contour in the upper (lower) half k plane for $x > (<) 0$. Any poles which crossed into the lower (upper) half plane as $\text{Im}\,\omega \to 0$ (and which remain inside the contour due to the deformation) correspond to growing instability waves in the "steady-state" response (see eq. (A.2)).

In short then, to obtain a causal solution, we need to obtain the transform of the solution to the initial value problem with the frequency having a large positive imaginary part. This solution will appear formally the same as if we were seeking a time harmonic solution from the start. Hence we can proceed from the time harmonic form while keeping in mind that the frequency has a large positive imaginary part. We then let $\text{Im}\,\omega \to 0$ and keep track of any poles in the k plane which cross the real axis and in this way obtain a causal solution for ω real.

A.3 Absolute Instabilities

It may happen that the analytic continuation just described cannot be carried out all the way to the real ω axis. One way this could occur is if two roots in the k plane, one originating in the upper and one in the lower half plane, merge for some complex ω with $\text{Im}\,\omega > 0$. As can be seen from figure A.3 the integration contour in the k plane will become "pinched" between the two poles and the deformation on which the analytic continuation rests cannot be performed. In these situations (as shown by Briggs and Bers) the asymptotic time response is dominated by a term which grows exponentially in time at every position in space and the flow is absolutely unstable.

When these absolute instabilities are present there is no "steady-state" and the concepts of spatial instability break down.

REFERENCES

1. Bers, A.: 1975, In Plasma Physics. Gordon and Breach.
2. Bogy, D.B.: 1979, Annu. Rev. Fluid Mech., vol. II.
3. Briggs, R.J.: 1964, Electron Stream Interaction with Plasmas. MIT Press.
4. Brown, S.N.; and Daniels, P.G.: 1975, J. Fluid Mech. 67, pp. 743-761.
5. Chandrasekhar, S.: 1961, Hydrodynamic and Hydromagnetic Stability. Oxford: The Clarendon Press.
6. Conway, J.B.: 1978, Functions of One Complex Variable. Springer-Verlag.
7. Crane, L.; Birch, S.; and McCormack, P.D.: 1964, Br. J. Appl. Phys. 15, pp. 743-750.
8. Crighton, D.G.; and Leppington, F.G.: 1974, J. Fluid Mech. 64, part 2, pp. 393-414.
9. Crighton, D.G.: 1985, Annu. Rev. Fluid Mech., vol. 17.
10. Donnelly, R.J.; and Glaberson, W.: 1966, Proc. Roy. Soc. London A., 290, (1423) pp. 547-556.
11. Drazin, P.G.; and Reid, W.H.: 1981, Hydrodynamic Stability, Cambridge Univ. Press.
12. Goldstein, M.E.: 1981, J. Fluid Mech. 104, pp. 217-246.
13. Jones, D.S.; and Morgan, J.D.: 1972, Proc. Cambridge Philos. Soc., 72, pp. 465-488.
14. Keller, J.B.; Rubinow, S.I.; and Tu, Y.O.: 1973, Phys. Fluids 16(12), pp. 2052-2055.
15. Kuhn, L.; and Meyers, R.A.: 1979, Sci. Am., 240 (4), pp. 162-178.
16. Lamb, H.: 1932, Hydrodynamics, Dover.

17. Landau, L.D.; and Lifshitz, E.M.: 1959, Fluid Mechanics, Pergamon Press.

18. Lee, H.C.: 1974, IBM J. Res. Dev. 18, pp. 364-369.

19. Lighthill, M.J.: An Introduction to Fourier Analysis and Generalized Functions, Cambridge Univ. Press.

20. Mattick, A.T.; and Hertzberg, A.: 1982, Acta Astronaut., 9, pp. 165-172.

21. McCarthy, M.J.; and Molloy, N.A.: 1974, Chem. Eng. J. (Lausanne) 7, pp. 1-20.

22. MorKovin, M.V.: 1969, Air Force Flight Dynamics Lab. Report AFFDL-TR-68-149.

23. Noble, B.: 1958, Methods Based on the Wiener-Hopf Technique for the Solution of Partial Differential Equations. Pergamon.

24. Pimbley, W.T.: 1976, IBM J. Res. Dev. 20, pp. 148-156.

25. Rayleigh, J.S.W.: 1978, Proc. Lond. Math. Soc. 10, pp. 4-13.

26. Rayleigh, J.S.W.: 1882, Philos. Mag. 34, p. 145.

27. Rienstra, S.W.: 1981, J. Fluid Mech., 108, pp. 443-460.

28. Roos, B.W.: 1969, Analytic Functions and Distributions in Physics and Engineering. Wiley.

29. Van Dyke, M.D.: 1964, Perturbation Methods in Fluid Mechanics, Academic Press.

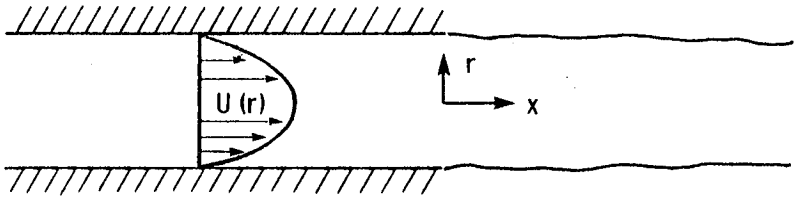

Figure 2.1- Flow geometry.

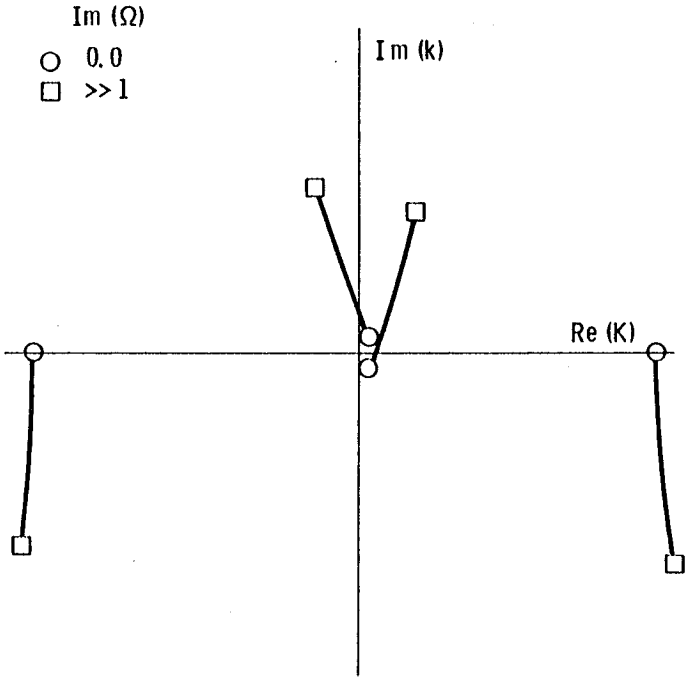

Figure 3.1- Movement of the roots of the Kernel function as ImΩ varies.

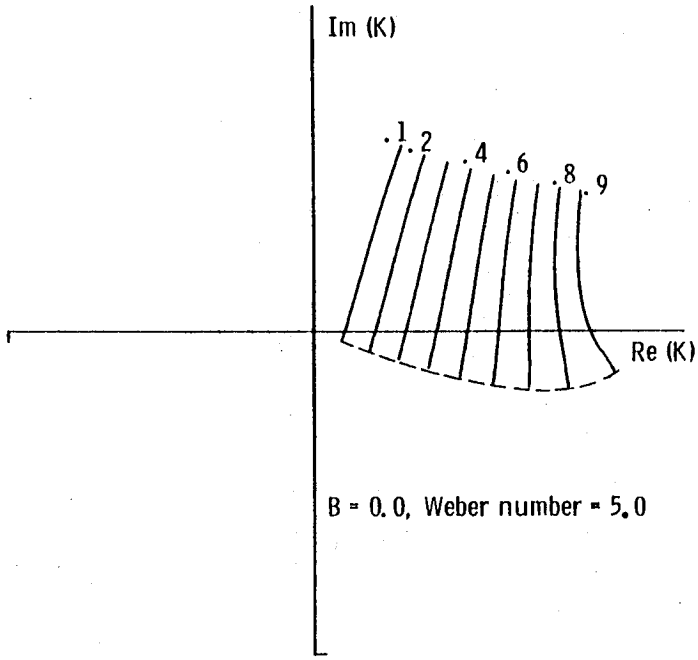

Figure 3.2 - Locus of complex root of χ for b = 0, β^2 = 5.

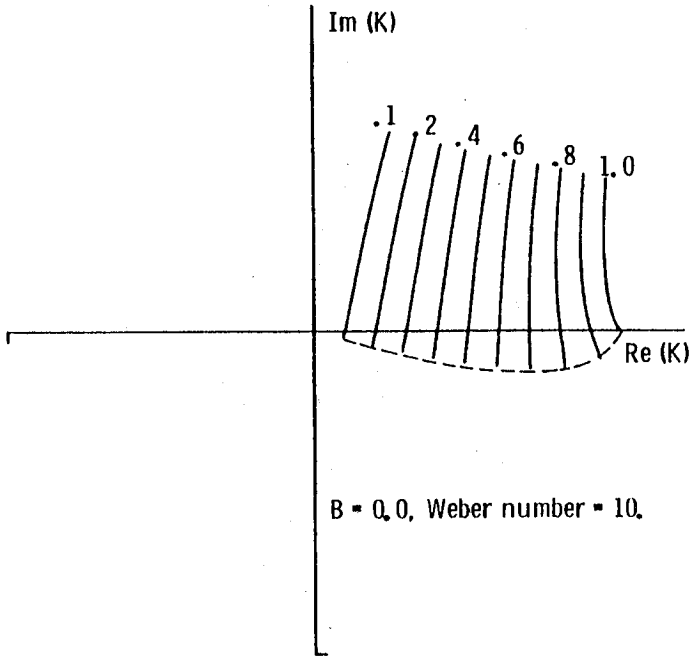

Figure 3.3- Locus of complex root of χ for b = 0, β^2 = 10.

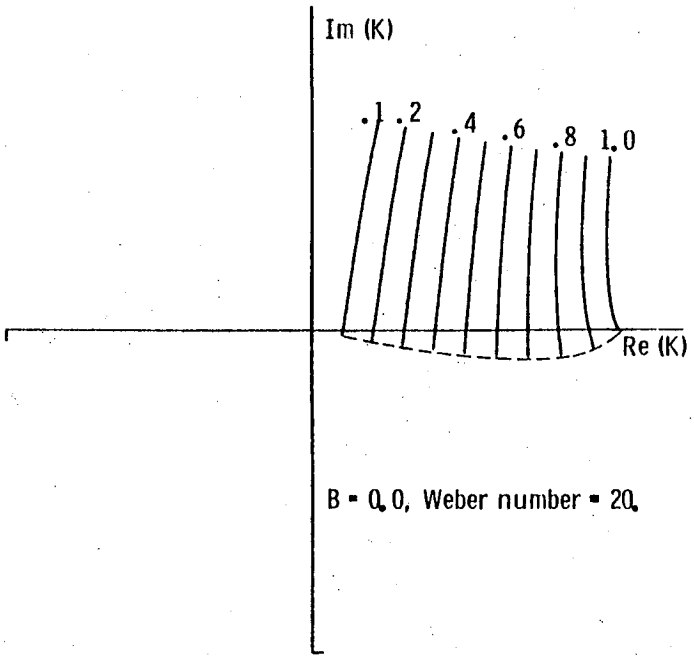

Figure 3.4 - Locus of complex root of χ for b = 0. β^2 = 20.

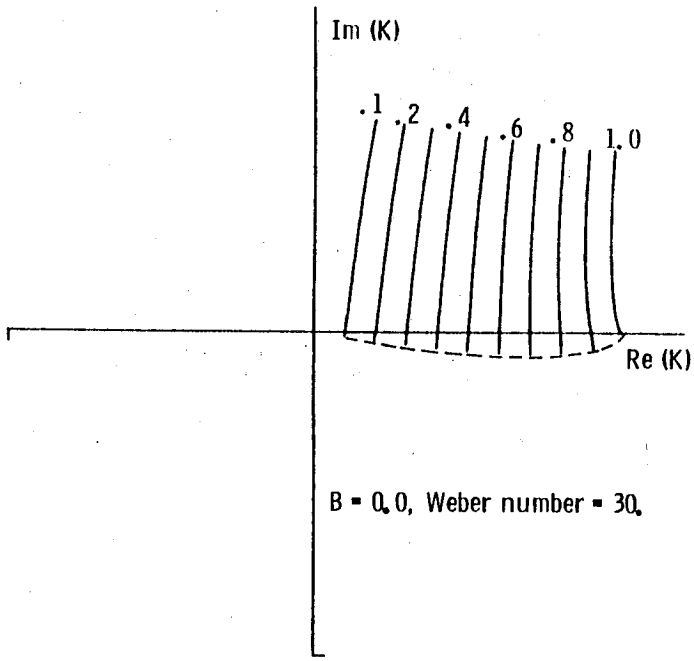

Figure 3.5– Locus of complex root of χ for b = 0, β^2 = 30.

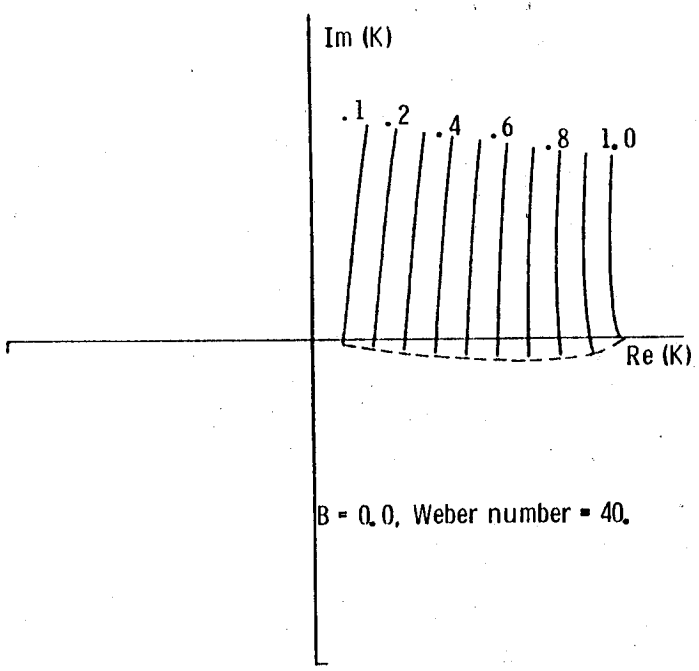

Figure 3.6 - Locus of complex root of χ for b = 0, β^2 = 40.

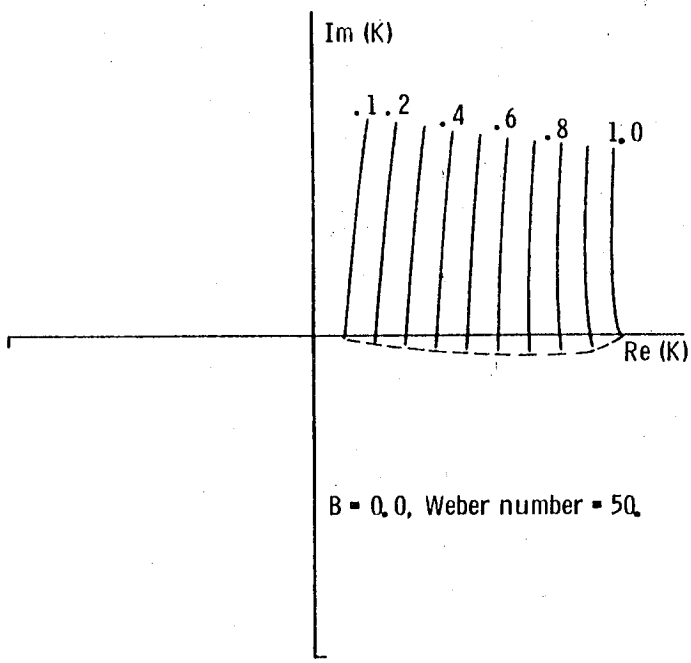

Figure 3.7 - Locus of complex root of χ for b = 0, β^2 = 50.

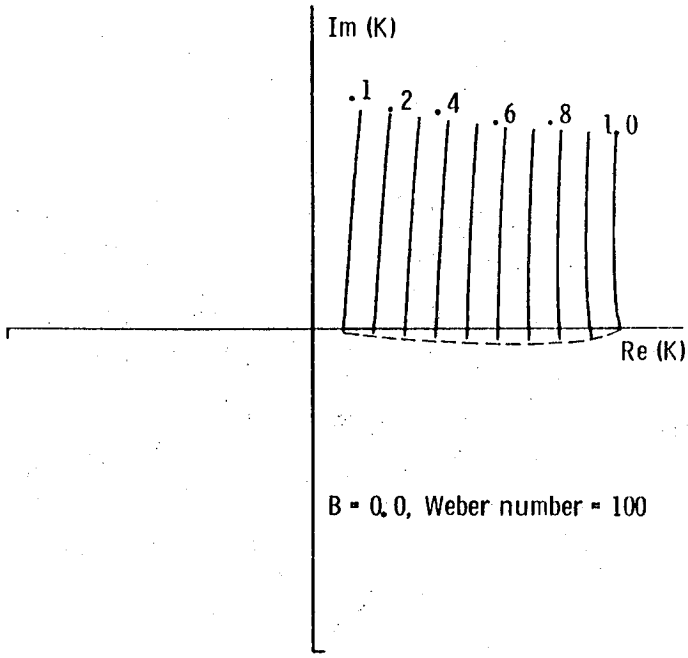

Figure 3.8 - Locus of complex root of χ for b = 0, β^2 = 100.

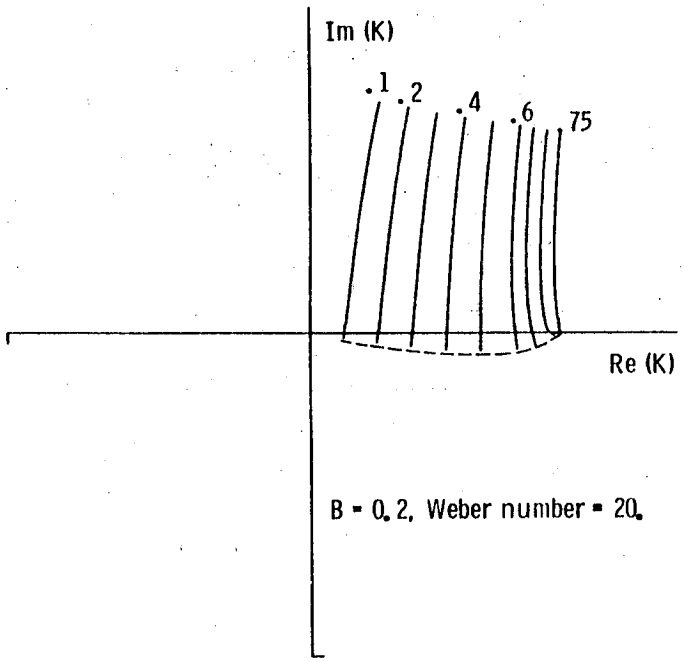

Figure 3.9 - Locus of complex root of χ for b = 0.2, β^2 = 20.

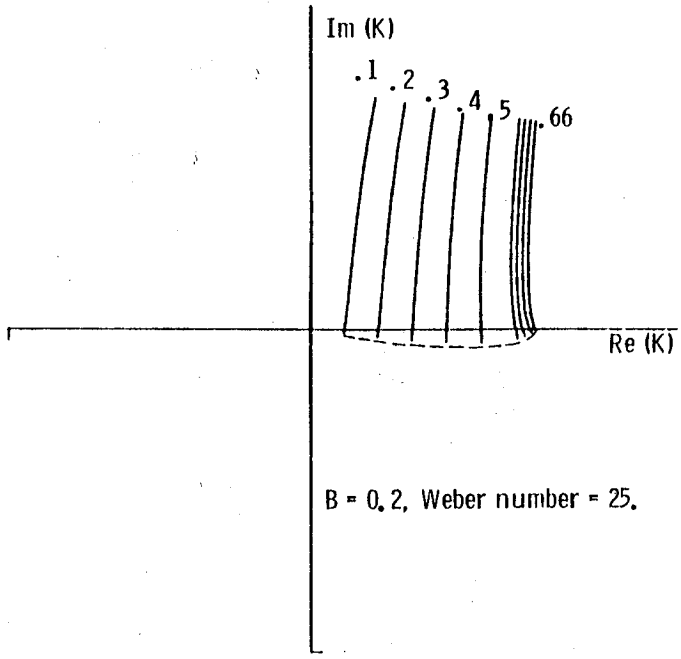

Figure 3.10 - Locus of complex root of χ for b = 0.2, β^2 = 25.

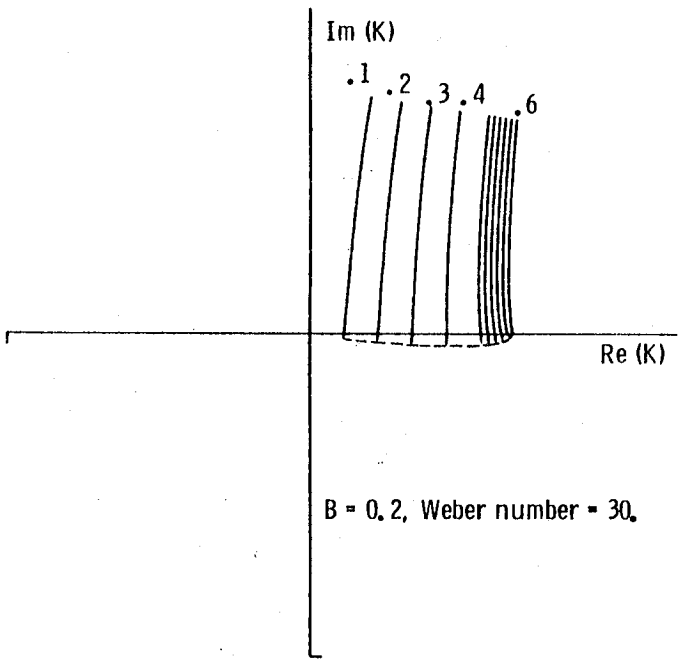

Figure 3.11 - Locus of complex root of χ for b = 0.2, β^2 = 30.

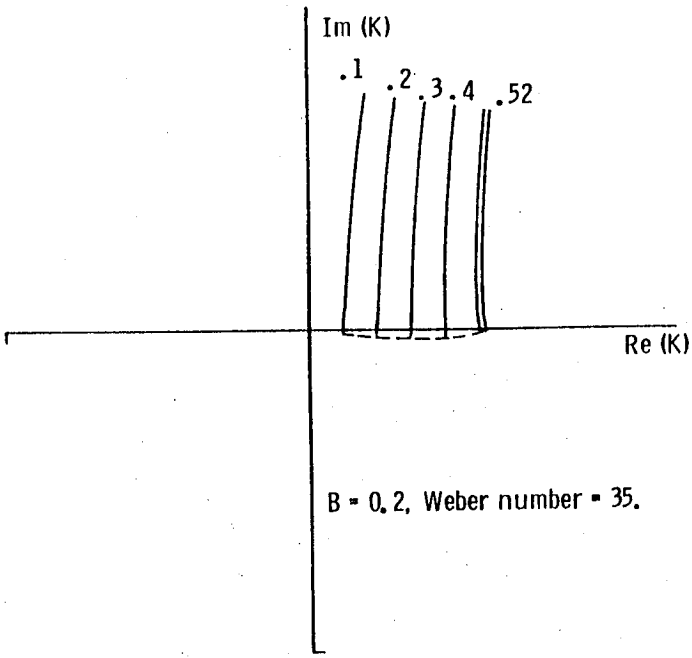

Figure 3.12 - Locus of complex root of χ for b = 0.2, β^2 = 35.

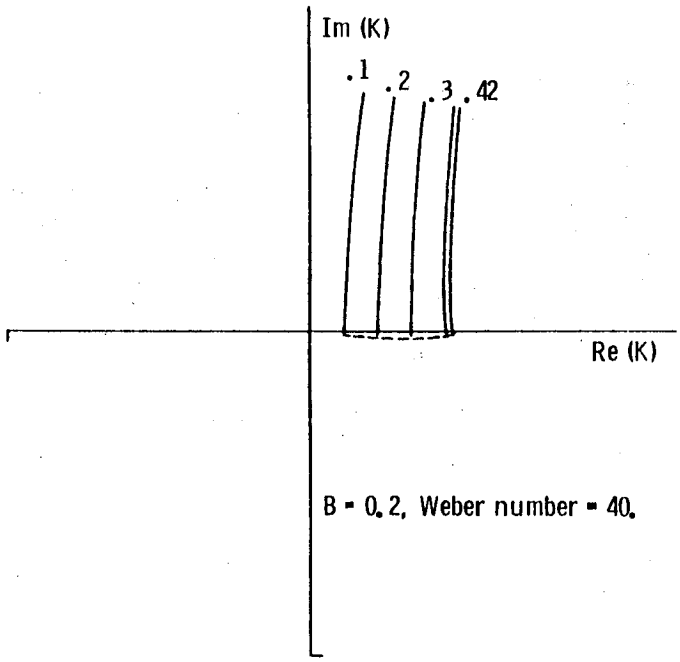

Figure 3.13 - Locus of complex root of χ for b = 0.2, β^2 = 40.

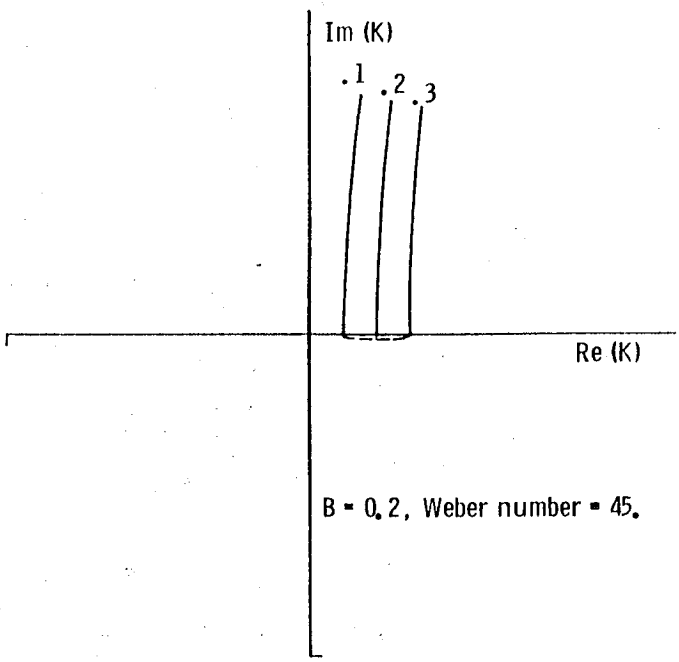

Figure 3.14 - Locus of complex root of χ for b = 0.2, β^2 = 45.

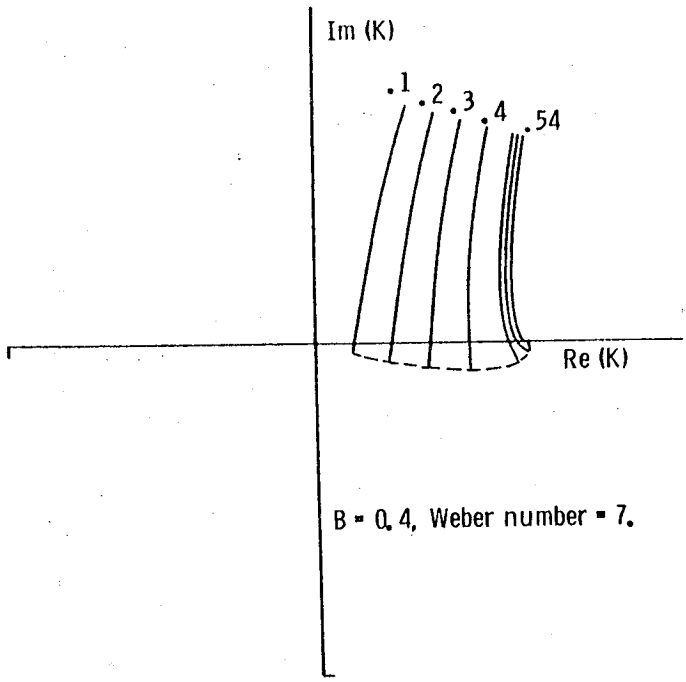

Figure 3.15 - Locus of complex root of χ for b = 0.4, β^2 = 7.

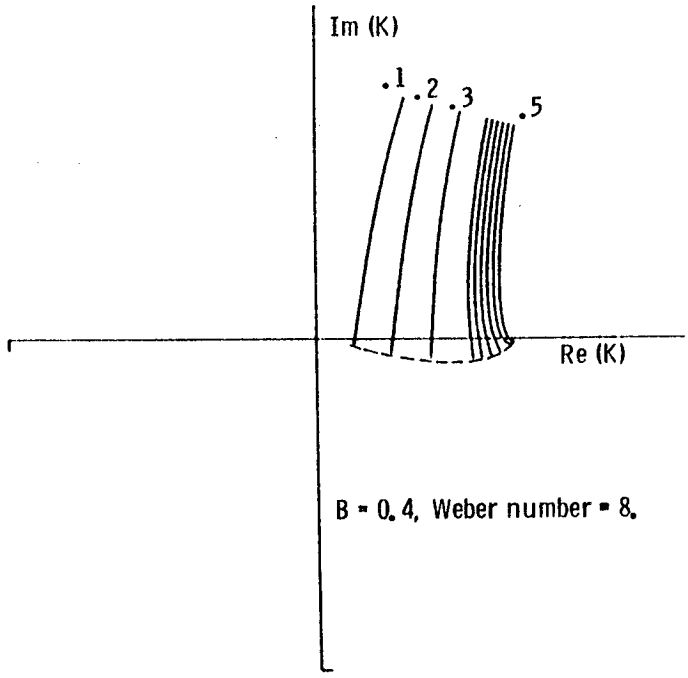

Figure 3.16 - Locus of complex root of χ for b = 0.4, β^2 = 8.

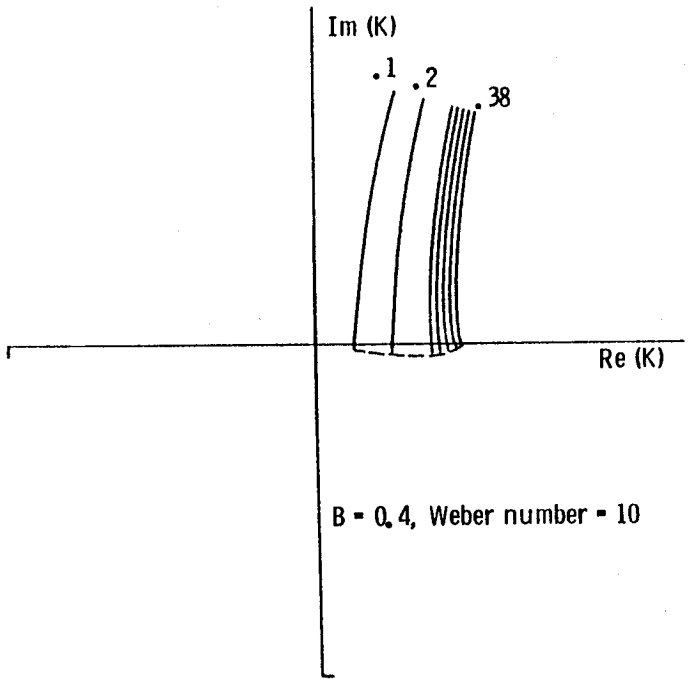

Figure 3.17 - Locus of complex root of χ for b = 0.4, β^2 = 10.

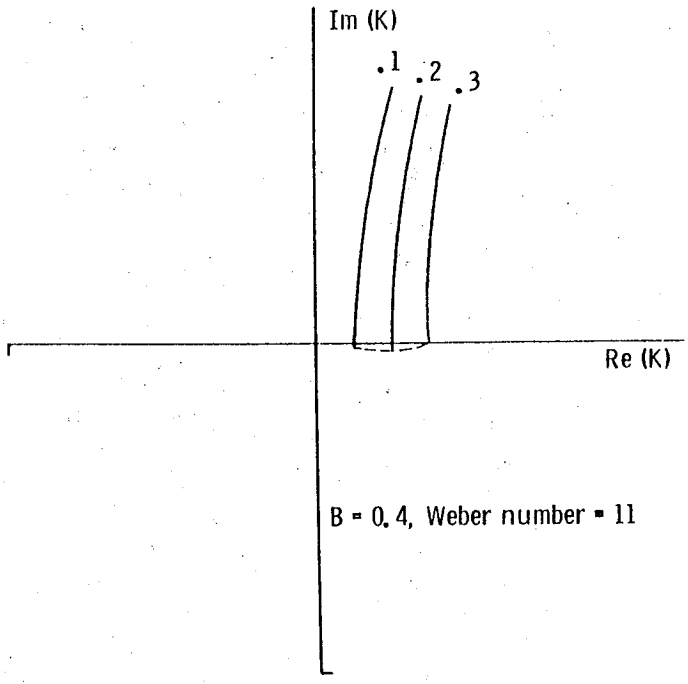

Figure 3.18 - Locus of complex root of χ for b = 0.4, β^2 = 11.

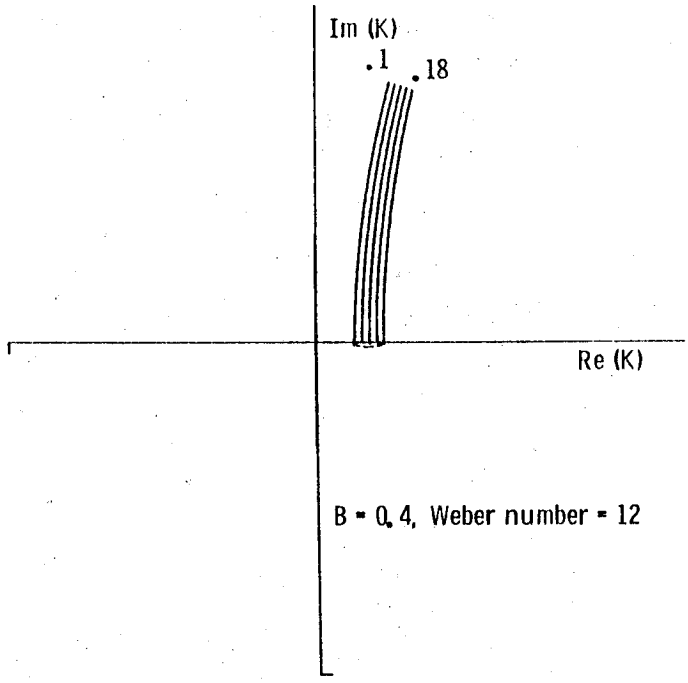

Figure 3.19 - Locus of complex root of χ for b = 0.4, β^2 = 12.

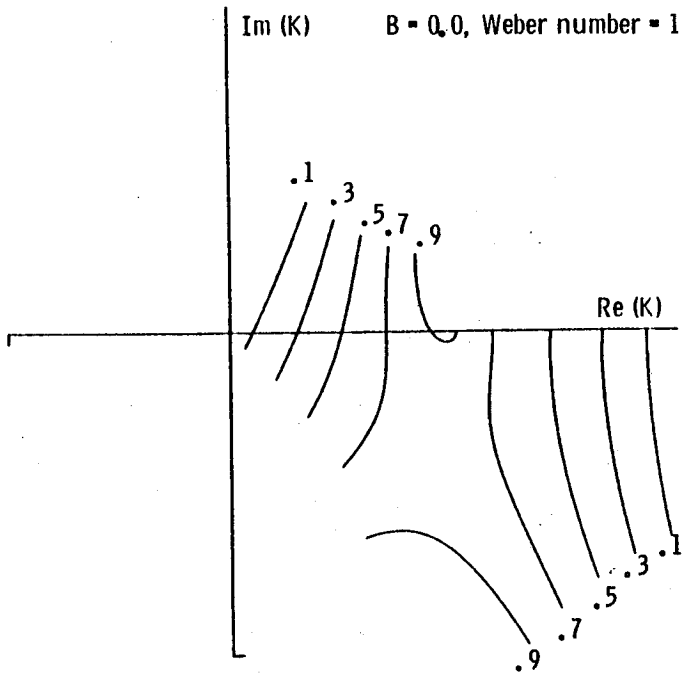

Figure 3.20 - Movement of roots of χ in the case of absolute instability.

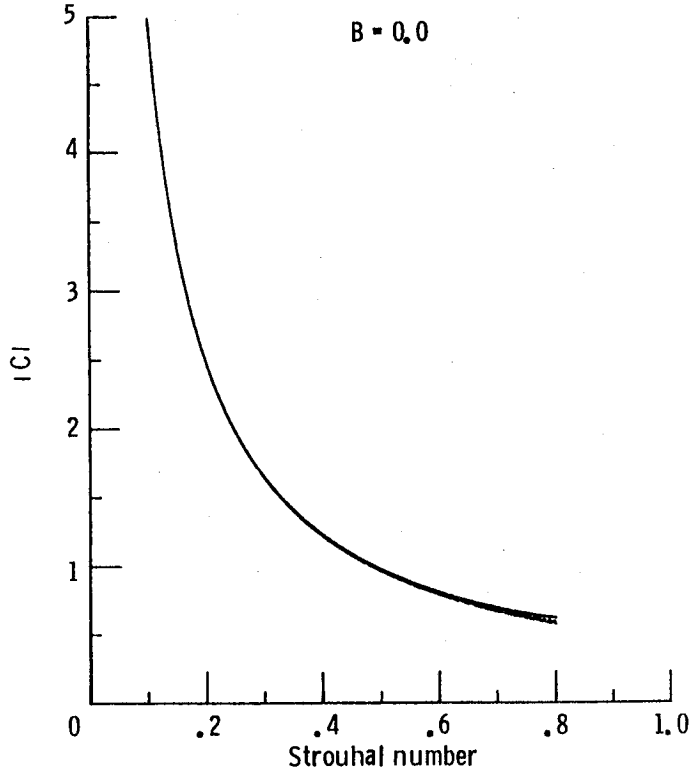

Figure 3.21 - Magnitude of the Coupling coefficient vs Strouhal number, b = 0, β^2 = 5, 10, 20, 30.

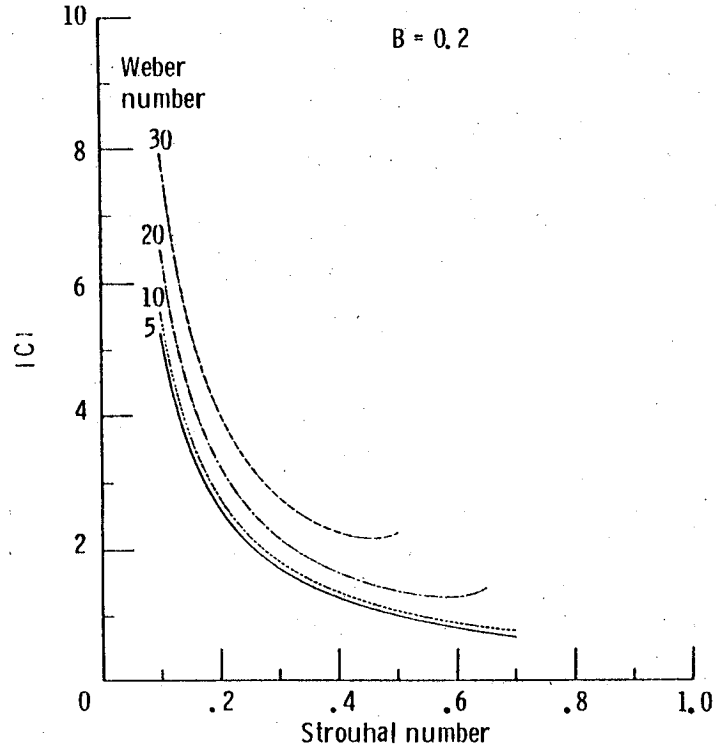

Figure 3.22 - Magnitude of the Coupling coefficient vs Stouhal number, b = 0.2, β^2 = 5, 10, 20, 30.

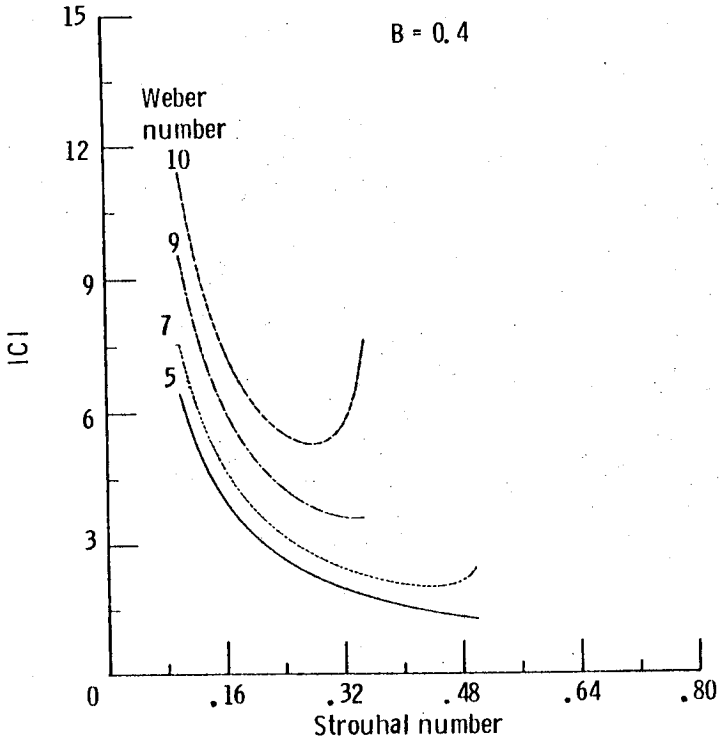

Figure 3.23 - Magnitude of the Coupling coefficient vs Strouhal number, b = 0.4, β^2 = 5, 7, 9, 10.

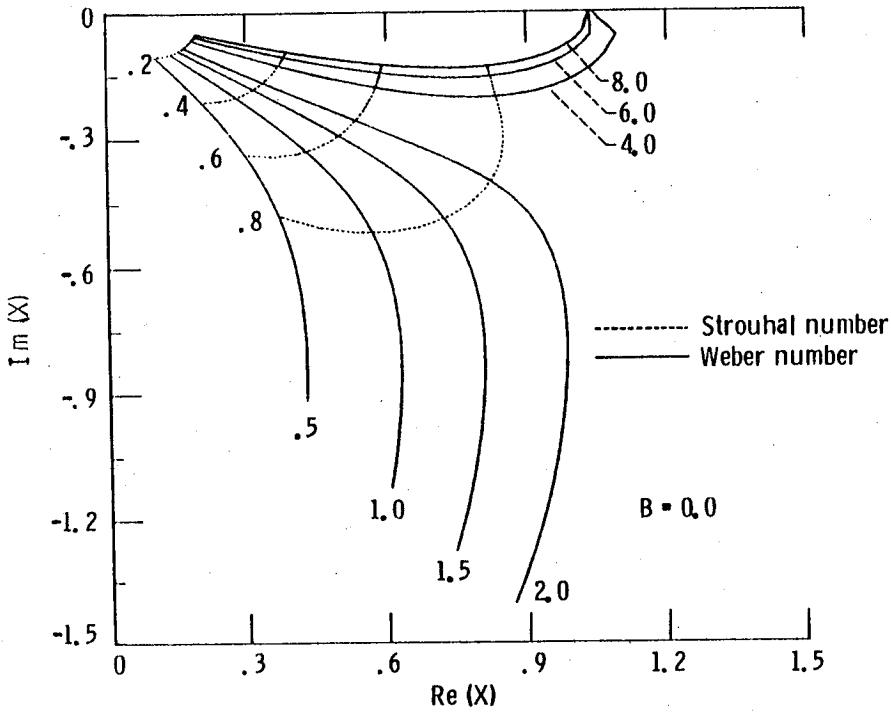

Figure 4.1 - Lowest order root of the dispersion relation, b = 0.

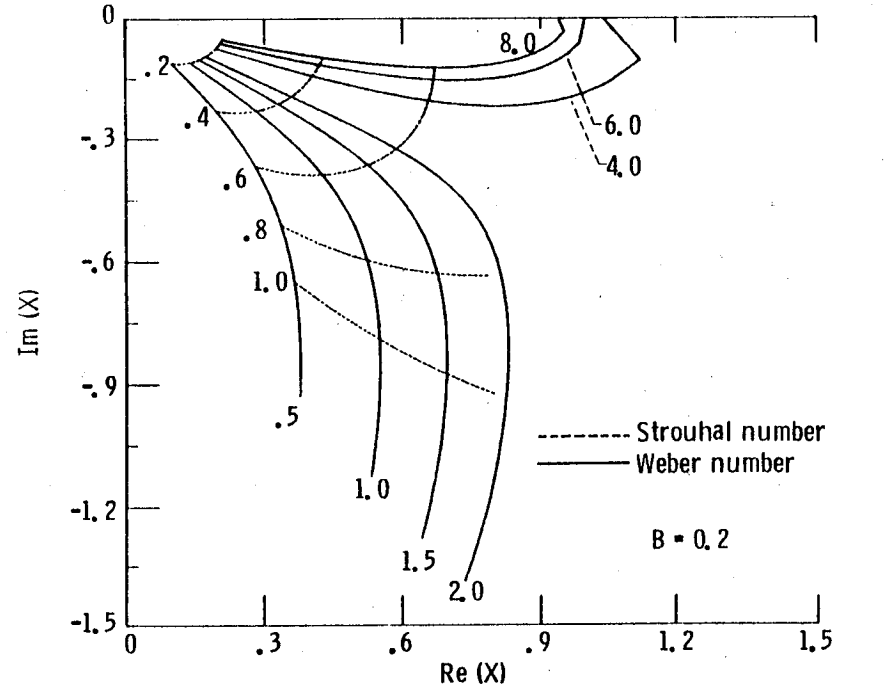

Figure 4.2 - Lowest order root of the dispersion relation, b = 0.2.

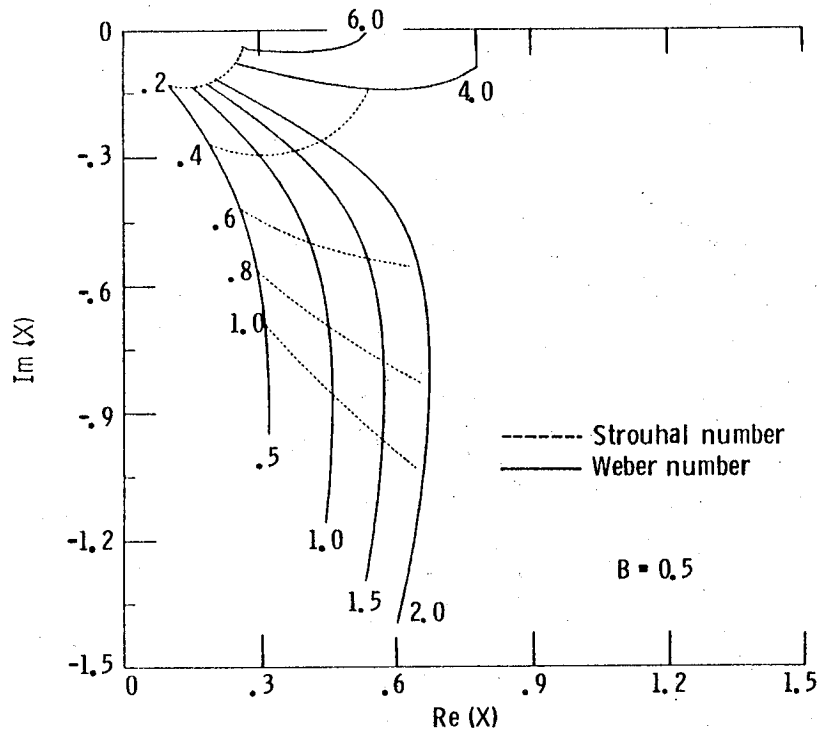

Figure 4.3 - Lowest order root of the dispersion relation, b = 0.5.

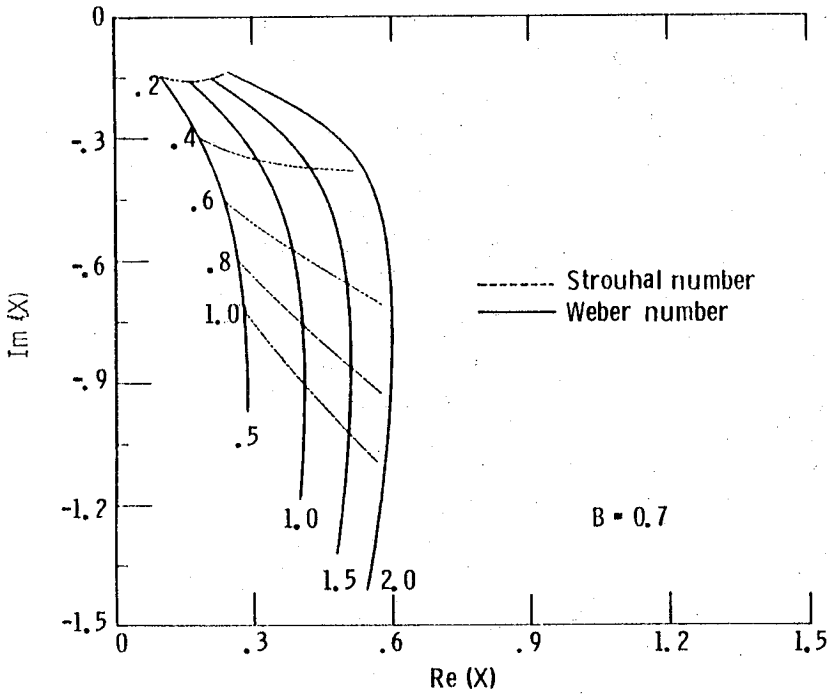

Figure 4.4 - Lowest order root of the dispersion relation, b = 0.7.

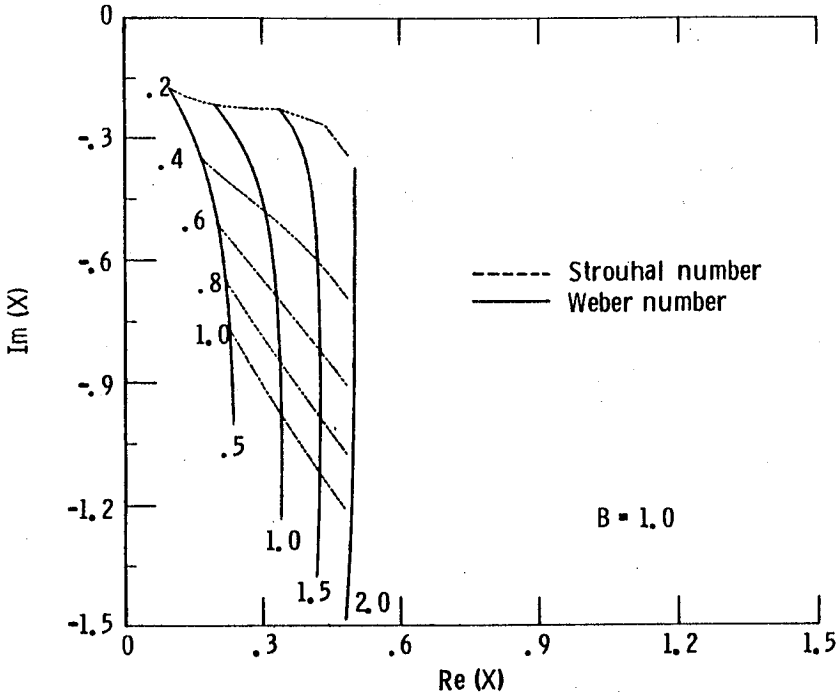

Figure 4.5 - Lowest order root of the dispersion relation, b = 1.0.

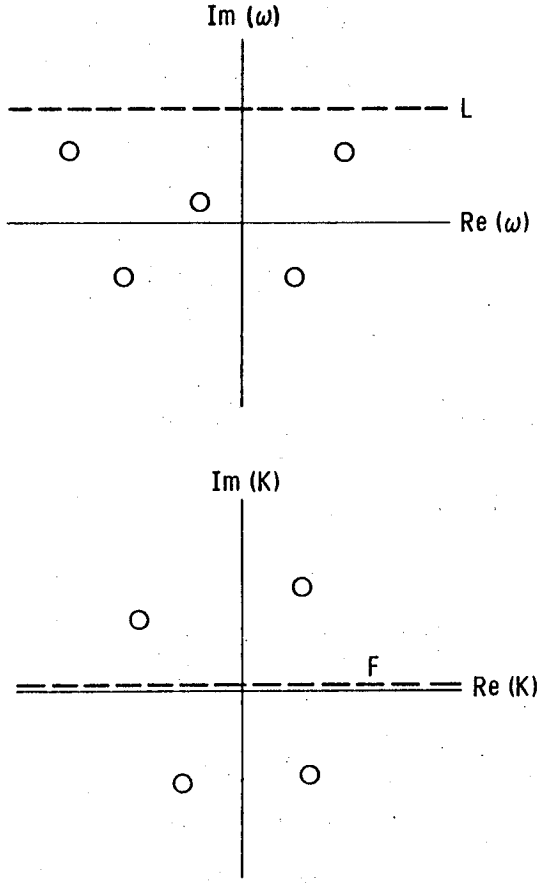

Figure A. 1 - Fourier inversion contours.

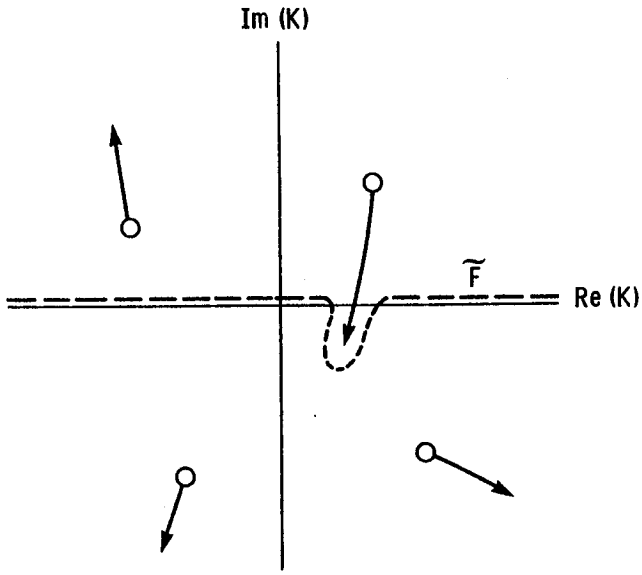

Figure A. 2- Movement of roots of dispersion relation for convective instability.

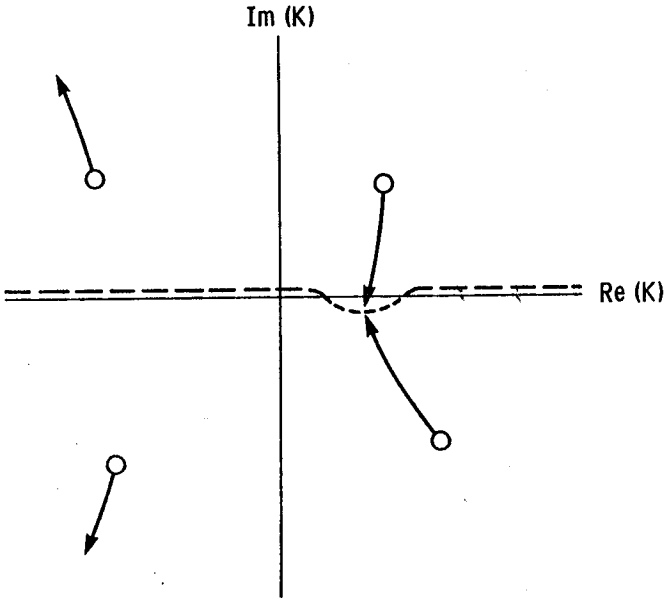

Figure A. 3- Movement of roots of dispersion relation for absolute instability.

1. Report No.	2. Government Accession No.	3. Recipient's Catalog No.
NASA TM-87041		

4. Title and Subtitle	5. Report Date
The Generation of Capillary Instabilities by External Disturbances in a Liquid Jet	6. Performing Organization Code: 506-36-22

7. Author(s)	8. Performing Organization Report No.
Stewart J. Leib	E-2503
	10. Work Unit No.

9. Performing Organization Name and Address	11. Contract or Grant No.
National Aeronautics and Space Administration Lewis Research Center Cleveland, Ohio 44135	13. Type of Report and Period Covered: Technical Memorandum

12. Sponsoring Agency Name and Address	14. Sponsoring Agency Code
National Aeronautics and Space Administration Washington, D.C. 20546	

15. Supplementary Notes

NASA Resident Research Associate from State University of New York at Buffalo; participant in the Integovernmental Mobility Program.
This report was a dissertation submitted to the Faculty of the Graduate School of State University of New York at Buffalo in partial fulfillment of the requirements for the degree of Doctor of Philosophy in June 1985.

16. Abstract

The receptivity problem in a circular liquid jet is considered. A time harmonic axial pressure gradient is imposed on the steady, parallel flow of a jet of liquid emerging from a circular duct. Using a technique developed in plasma physics a causal solution to the forced problem is obtained over certain ranges of Weber number for a number of mean velocity profiles. This solution contains a term which grows exponentially in the downstream direction and can be identified with a capillary instability wave. Hence it is found that the externally imposed disturbances can indeed trigger instability waves in a liquid jet. The amplitude of the instability wave generated relative to the amplitude of the forcing is computed numerically for a number of cases.

17. Key Words (Suggested by Author(s))	18. Distribution Statement
Hydrodynamic stability Receptivity Liquid jets	Unclassified - unlimited STAR Category 34

19. Security Classif. (of this report)	20. Security Classif. (of this page)	21. No. of pages	22. Price*
Unclassified	Unclassified		

*For sale by the National Technical Information Service, Springfield, Virginia 22161